Journal of Humanitarian Engineering

Volume 9, Issue 1
ISSN 2200 4904

JOURNAL OF HUMANITARIAN ENGINEERING

engineers without borders australia

Journal of Humanitarian Engineering (JHE)

The Journal of Humanitarian Engineering (JHE) is an open access publication that publishes outcomes of research and field experiences at the intersection of technology and community development. The field of "humanitarian engineering" describes the application of engineering and technology for the benefit of disadvantaged communities. The field spans thematic areas from water to energy to infrastructure; and applications from disability access to poverty alleviation. The JHE aims to highlight the importance of humanitarian engineering projects and to inspire engineering solutions to solve the world's most pertinent challenges.

For more information, visit: www.ewb.org.au/journal.

INDIGENOUS AUSTRALIAN ACKNOWLEDGEMENT

EWB respectfully acknowledges the Traditional Owners of the Country on which we work.
To learn more about our commitment to reconciliation, read EWB's Reconciliation Action Plan.

INDEXED IN DOAJ

Cover photo:
Türkiye earthquake, by European Commission (Barbaros Kayan) - Audiovisual Service, Attribution, https://commons.wikimedia.org/w/index.php?curid=128687843

JOURNAL OF
HUMANITARIAN
ENGINEERING

GUEST EDITORIAL

I am honoured to introduce this volume in a guest editorial for the Journal of Humanitarian Engineering, offering some reflections on where the field of humanitarian engineering might focus its attention given recent events.

Scenes from the recent (2023) Türkiye and Syria earthquakes seem all too familiar, hardly distinguishable from Kashmir (2005), Sichuan (2008), Haiti (2010), and others. The level of destruction is no less shocking. In Türkiye, its government estimates that more than 850,000 buildings were damaged or destroyed. Engineers are yet again being called into action to respond – the scale of which requires a massive level of coordination to deliver the solutions and services to meet basic needs. We should continue to rigorously support these efforts, including documenting evidence of how to build back safer. Simultaneously, we need to be asking how can such scale of devastation happen and what were the missteps to arrive here (yet again)?

While field investigations will document shortcomings and provide new recommendations to reduce earthquake risk, the engineering knowledge required to avoid the immense loss of life largely existed beforehand. Like other disasters, the dilemma wasn't about missing requisite knowledge to save lives, but rather mobilising it. Rather this disaster, like so many others, was the result of accumulating social and political factors. Assuming that engineering does not have a role to play in addressing these problems – offering only technical fixes – would be a mistake.

The engineering field often markets itself as being apolitical and neutral – the uncomfortable reality is engineering practice is intertwined with enacted governance with unequal power dynamics at play. Humanitarian engineering offers a pathway to engage with these ethical dilemmas that can address or reinforce marginalisation. So, what needs to change?

First, we as engineers need to lean into advocacy. Engineers need to recognise that our role offers the opportunity to represent marginalised voices to create positive social change. Unless we become active in the political processes that create disasters, we're likely to repeat our failures. Interviews our team have conducted with humanitarians that have

worked in Syria on sheltering solutions have highlighted that one of the largest challenges is negotiating the space to do the needed work amidst complex and competing government interests. We need to consider not just the constraints of users in our designs, but also the political environments in which solutions are implemented. The good news is we're getting better at this – both in shifting the educational paradigm to prepare engineers for this type of work and through engineering professional societies' activism.

Second, as a research community, we need to mobilise the decades of knowledge we are collecting. It isn't enough to just document lessons, we need to be active in making knowledge more accessible. This means communicating consequences and allowing communities to make risk-informed decisions. To do this, we need to view the engineering profession as more than just the products we make. We should be placing renewed value on co-creating knowledge with communities – working at the interface between scientific and local knowledge. The process we take as engineers to reach solutions has the potential to either reinforce inequities or provide a platform for larger change.

Engineers have a critical role to play in reducing disaster risk, but only if we examine our positionality in the processes that create disasters.

Dr Aaron Opdyke
Senior Lecturer in Humanitarian Engineering
The University of Sydney

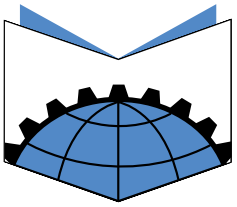

JOURNAL OF
HUMANITARIAN
ENGINEERING

Journal of Humanitarian Engineering

Volume 9, Issue 1

ISSN 2200 4904

CONTENTS

Is there a case for gridshell structures in humanitarian assistance and disaster relief efforts?

Thomas B. Imhoff
Graduate, Mechanical Engineering Department
United States Naval Academy
tbi20@cam.ac.uk

Samar R. Malek
Associate Professor, Mechanical Engineering Department
United States Naval Academy
malek@usna.edu

ABSTRACT: *This article focuses on the core concerns of shelter and settlement, and more specifically focuses on large-span shelters in humanitarian assistance and disaster relief (HA/DR) efforts. Furthermore, this article introduces the audience to novel large-span structures called gridshells. This paper presents a parametric, computational study that quantifies the efficacy of bracing orientation and arrangement on the load carrying capacity of gridshells. The varied parameters include the grid density ("16 by 16" to "30 by 30") and the bracing scheme (unbraced, continuous fully-braced, discontinuous fully-braced, continuous half-braced, and discontinuous half-braced). Four load cases were analyzed, namely a symmetric distributed load, an asymmetric distributed load, a centered point load, and an off-centered point load. The results of the study provide designers with trends and basic design options upon which they can base further analysis depending on the requirements of the final structure.*

KEYWORDS: *Humanitarian assistance, Disaster relief, Shelter, Gridshells, Parametric studies, Bracing, Buckling*

1 INTRODUCTION

Humanitarian assistance and disaster relief (HA/DR) efforts generally comprise three distinct phases following a disaster strike: response, recovery, and restoration (Disaster Response in Asia and the Pacific 2013). The response phase lasts for approximately two weeks following the initial disaster. Throughout this period, search and rescue operations are prevalent and necessities such as food, water, and shelter are points of focus. The recovery phase follows the initial response phase and generally lasts between one and twenty weeks. Hallmarks of the recovery phase include establishing basic local services such as hospitals, housing, sanitation, and more. Robust family shelter construction also begins during this period. Finally, the recovery phase marks the transition from a disaster relief situation to more stable, post-disaster existence. The entire timeline often takes place over many months, though it is common for the recovery phase to last longer. Furthermore, modern crises have a higher likelihood of becoming a protracted crisis, stretching the typical timeline from months to years. Perhaps the most poignant example of a protracted crisis is the global refugee crisis which sees nearly 80 million people displaced (Figures at a Glance 2020). These crises force populations to relocate entirely, often erasing the possibility of a true restoration period, instead resulting in an indefinite state of stifled recovery.

The generic timeline for HA/DR is of course an oversimplification of highly complex and fluid response efforts, yet the outline still serves as an adequate roadmap. The disaster relief timeline indicates that after the initial response period, the recovery period focuses on establishing better small-scale structural solutions for family accommodations, as well as some community services. While vitally important, this focus neglects larger structural solutions aimed at facilitating community gathering. Large-span structures are highly important to city planning because they accommodate and encourage community cohesion. Even in temporary settlements, large-

Figure 1: *ZA Pavilion, fully constructed in Cluj, Romania* (*Photo by Dragos Naicu*)

community cohesion. Even in temporary settlements, large-span shelters are necessary because of the physical space required for religious services, leisure, educational activities, industry and business, and community gatherings. Beyond the physical requirements for space, large-span shelters support community fellowship, an extremely important aspect of mental and emotional health (Project for Public Spaces 2018).

There are no purpose-built, large-span structures currently used for HA/DR. This non-availability is likely due to a lack of understanding of their importance, a focus on establishing other comforts for impacted populations, and a lack of adequate structures to fit this need. Structures such as durable expeditionary tents, shipping container structures, and ready-made deployable structures have characteristics that can make them advantageous for use in HA/DR scenarios, yet when it comes to large-span shelter, each is quite limited (Concrete Canvas Limited 2018, Edilsider 2020, Operator's and Unit Maintenance Manual 1999).

This paper introduces gridshells as a potential solution. Gridshells are a type of shell structure that can be used as a temporary shelter. Gridshells are spatial shells made of an initially flat, structural lattice that is subsequently bent onsite into a doubly curved surface for shelter. Gridshells are most popular in Europe as architectural centrepieces and atrium enclosures, yet their potential stretches beyond these applications. Research indicates that gridshells constructed from long, thin pieces of timber are extremely effective in providing large-span shelter. The ZA Pavilion in Cluj, Romania demonstrated that a self-supporting 12 m by 18 m pavilion could be constructed using only hand tools and a volunteer workforce, see Fig. 1 (Naicu, Harris, & Williams 2014).

When designed with HA/DR in mind, gridshells are highly portable because they require no heavy machinery for construction and can be packaged neatly in standard shipping containers. The structures are also highly sustainable due to their natural construction, modular and replaceable parts, and ability to be assembled and disassembled numerous times. This paper shows that the shells themselves are structurally efficient by design and maintain durability and strength under extreme loading conditions caused not only by wind and precipitation, but also by asymmetric loads such as children climbing on the structure or patrons hanging belongs underneath.

In addition to their many engineering accolades, gridshell structures are inherently beautiful, an attribute often overlooked in HA/DR efforts when the focus is on basic survival. After the initial response period, beauty can become an important factor during the recovery period to facilitate rehabilitation. Humans naturally seek that which is pleasing to the eye, often subconsciously. Providing beauty and balance amidst a crisis, however small, can have large impacts on the mental and emotional health of those affected by trauma.

2 PROBLEM STATEMENT

Completed in 1975, Frei Otto's Mannheim Multihalle was one of the first freestanding large-span gridshells designed as an enclosure for public events (Happold & Liddell 1975). Since then, gridshells have been used as pavilions and atriums in structures such as the British Museum, the Palacio de Comunicaciones, the Dutch Maritime Museum, and others (Sischka 2000, Schlaich et al. 2009, Adriaenssens et al. 2009). During the design of these structures, the primary concern was failure due to global buckling, often

the dominant failure mode for gridshells (Knippers & Helbig 2009). Global buckling occurs when an entire structure collapses at once, rather than a single part of the structure experiencing failure. While these structures have been extremely successful, gridshell technology holds the potential for use in the broader built environment beyond these niche applications.

In order to adapt the structures for new applications, additional research must investigate how these structures perform under asymmetric load cases, in a broad sense, and how bracing can improve their structural performance. Symmetric loads are very common in engineering practice, while asymmetric loads are less commonly dealt with when designing gridshells. A symmetric load can be thought of as a balanced load that affects the entire structure in the same manner, while an asymmetric load is unbalanced. Bracing is widely used to stiffen gridshells; however, little research has investigated the extent to which bracing placement and orientation affects structural performance under both symmetric and asymmetric loads (Naicu, Harris, & Williams 2014). This paper aims to establish trends associated with gridshell performance under these circumstances in order to inform design decisions.

3 METHODOLOGY

The research methodology, based on previously employed methods, focuses on developing a viable candidate structure to act as a basis for parametric variations (Malek, Wierzbicki, & Ochsendorf 2014). The results are validated numerically, using an independent finite element analysis (FEA) software, because closed-form analytical solutions are currently impossible to generate and experimental verification was not possible with available resources.

3.1 Design of Candidate Structure

The general features of the candidate structure are fixed, while geometric properties such as grid density and bracing are varied. Grid density refers to the number of grid spaces that comprise the lattice and bracing refers to the elements added to stiffen the lattice. Higher grid densities result in a "finer" lattice mesh pattern.

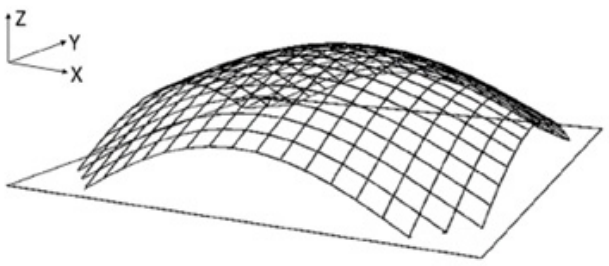

Figure 2: *The candidate gridshell structure with a clipped square grid and three distinct touchdown points per corner*

The candidate gridshell features a 15 m "clipped-square" grid with four corner supports, see Fig. 2. Each corner support is comprised of three distinct touchdown points per corner, helping to alleviate high compressive forces near the boundaries. High compressive forces near the boundaries cause the wooden beams near these locations to break, leading to structural failure when less than three distinct points are used. The entrance arches on each side (four in total) are fixed at a height of 2 m. The maximum height at the centre of the shell fluctuates due to the geometric variations but ultimately falls between 4 m and 5 m.

The material properties assigned to the structure mimic those of common timber species (Young's modulus of 105 MPa and yield strength of 0.13 MPa). The member cross-section is set at 70 mm wide and 30 mm thick. Together, these properties and dimensions describe a thin wooden beam that is flexible and can bend considerably without breaking. The gridshell is modelled using what is known as the continuous lattice assumption. This assumption is merely a simplification used to streamline the analysis and states that a single layer gridshell can be modelled with all its beams in one continuous plane. A single layer gridshell is actually made up of two layers of stacked beams, and the joints have their own unique stiffness. This naming convention is slightly misleading, as a single layer gridshell is made up of two layers of beams. However, two layers of crossed beams are required to create a single lattice, hence the nomenclature. Because this model assumes that the lattice lies in one continuous plane, rather than two stacked planes, the joints are modelled as having the same stiffness and material properties as the rest of the lattice, in this case, wood. Despite these assumptions, a continuous lattice shell and a true single layer shell exhibit the same overall trends and yield results within 15% of one another (McCormick et al. 2003). This study seeks to illuminate trends and suggest near-final designs for gridshells; therefore, this margin of error is acceptable. Once a final design is selected, a higher fidelity model should be used to verify performance prior to construction.

3.2 Parametric Variation

During the parametric study, the grid density varies from "16 by 16" to "30 by 30." Five bracing schemes are analysed: unbraced, continuous fully-braced, discontinuous fully-braced, continuous half-braced, and discontinuous half-braced. The bracing schemes are defined as "half" or "full," depending on whether all or only half of the grid squares are braced, and "continuous" or "discontinuous" depending on whether the additional members brace one or more than one cell, see Fig. 3. The cross section, support conditions, and entrance arch height are held constant.

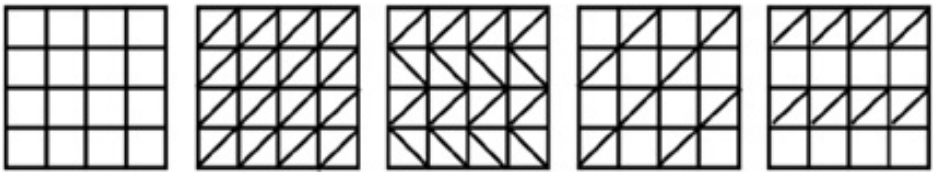

Figure 3: (*left to right*) *Bracing layouts – unbraced, continuous fully-braced, discontinuous fully-braced, continuous half-braced, discontinuous half-braced*

Figure 4: (*left to right*) *Load cases – symmetric distributed load, asymmetric distributed load, centred point load, off-centred point load*

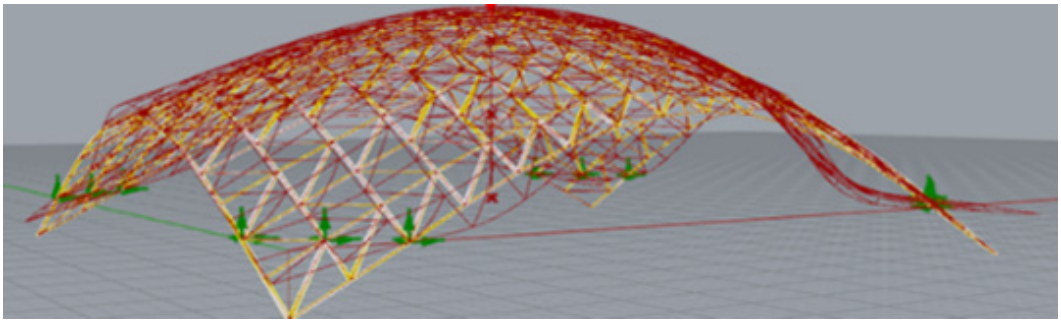

Figure 5: *Lowest buckling mode failure of a "20 by 20", discontinuous half-braced shell under a centred point load*

Each iteration of the structure is subjected to four load cases: a symmetric distributed load, an asymmetric distributed load, a centred point load, and an off-centred point load, see Fig. 4.

4 RESULTS

Taken as a large data set, the results of the parametric variations demonstrate how the shell performs under various loading scenarios and how different bracing schemes impact its performance. The failure mode studied in each iteration is global buckling, specifically the lowest buckling mode. A nonlinear, large deformation analysis is utilized to analyse each structure. This type of analysis iterates structural deformation as the solution converges, thereby mimicking real behaviour more closely than a first order, linear analysis. The buckled behaviour of the shells varies slightly based on the applied load case. Figure 5 shows an example of global buckling failure of a "20 by 20", discontinuous half-braced shell subjected to a centred point load. Note that the buckled shell is superimposed over the unbuckled shell.

4.1 Symmetric Distributed Loads

In the built environment, gridshells are likely to encounter symmetric distributed loads such as self-weight, cladding weight, and precipitation loads. These loads affect the entire structure in a balanced and distributed manner. When subjected to symmetric distributed loads, the strength of the structure varies primarily with bracing scheme. As expected, additional bracing material improves structural performance. Adding a half-braced scheme to the shell improves load carrying capacity by an average of 27%, for a 34% increase in weight compared to the unbraced shell. Similarly, the maximum load carrying capacity of the fully-braced shell shows an average increase of 53%, for a 66% increase in weight, compared to the unbraced shell. In both cases, every 1.0% increase in strength is associated with a 1.25% increase in weight. Increasing the grid density has little effect on the shell's strength and accounts for only small improvements in structural performance.

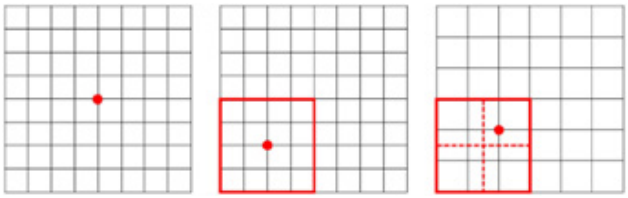

Figure 6: (left to right) Point load application – centred, off-centred (true), off-centred (closest).

4.2 Asymmetric Distributed Loads

In addition to symmetric distributed loads, gridshells are likely to encounter asymmetric distributed loads in the form of wind pressure or unequally affixed cladding. These loads are distributed over a large area but affect the structure in an unbalanced manner. This load case is defined as a load applied evenly over one half of the structure, thereby creating an asymmetric distributed load. Once again, global buckling failure dominates the structural response compared to local buckling. Additional bracing improves the load carrying capacity of the shell similar to a gridshell subjected to a symmetric distributed load, see above. Increasing the grid density under this loading scheme results in a loss of strength and worse performance.

Point Loads

Gridshells can be subjected to point loads when items are hung from shells' joints or individuals climb atop the shells for maintenance. Point loads are concentrated in a single location rather than spread over a large area. A centred point load is applied at the central intersection of the structural lattice. An off-centred point load is applied in the centre, or nearest centre, of a single quadrant of the structural lattice. If a central node is not present within the quadrant, the next closest node to the centre of the structure itself is used as the load application point, see Fig. 6.

Subjected to either of the point loads, the strength of the shell improves as grid density increases. Furthermore, any additional bracing also improves the shell's performance, regardless of the type of point load.

4.3 Continuity

This section takes a holistic view of the results of each of the load cases to understand how the continuity of bracing schemes affects structural performance. Considering fully-braced shells, the continuity of the bracing did not have a significant impact on structural performance. Both continuous fully-braced schemes and discontinuous fully-braced schemes consistently produce results within 10% of one another for all types of applied loads. However, continuous half-braced schemes consistently exhibit better performance (10 out of 12 cases), regardless of load case or grid density, than discontinuous half-braced layouts.

5 APPLICATION OF RESULTS

The results of the study yield trends describing the behaviour of a small gridshell under various load cases as grid density and bracing scheme are altered. These trends serve as a design guide to adapt gridshells for broader use. There is not a "one size fits all" solution when it comes to gridshell design. For example, improving the shell's failure resistance with respect to asymmetric loads can be brought about by decreasing grid spacing, yet improving the shell's failure resistance with respect to point loading requires the opposite. Furthermore, the strongest shell in an absolute sense might weigh too much for its intended application. As a result, the data must be interpreted based on the characteristics most important to the problem at hand.

In this paper, the results are used to help develop a mobile pavilion for HA/DR. Current products marketed as deployable pavilions weigh between 50 N/m^2 (large, lightweight tents) and 600 N/m^2 (ready-made concrete structures) (Operator's and Unit Maintenance Manual 1999, Concrete Canvas Limited 2018). As a result, a weight competitive structure might fall between 50 N/m^2 and 75 N/m^2. In this study, grid densities between 18 and 22 fit that weight category. Within these regions, ideal performance zones can be specified based on the demands placed on the structure. In this case, relevant building codes such as the International Building Code and Sphere Handbook are used to determine the limiting load cases. For this structure, the Attica region of Greece is used to calculate wind and precipitation loads.

Note that in Fig. 7, the ideal performance zones for an HA/DR application are indicated with boxes. An ideal shell falls within the box. Performance beneath the box is unsafe and performance above the box is superfluous. The red markers on the graphs represent a continuous half-braced gridshell with a grid density of 20. This is one of the grid densities tested with a continuous half-braced scheme, and it consistently outperformed the discontinuous half-braced scheme with the same grid density.

In this example, discontinuous half-braced and continuous half-braced schemes both fall within the ideal performance zones, while both fully-braced schemes fall within or above those same regions. For the same amount of material, the continuous half-braced scheme applied over a gridshell with a grid density of 20 outperforms its discontinuous counterpart. Additionally, continuous bracing is easier to install on the structure during the construction process compared to discontinuous bracing, representing an additional advantage. As a result, a 15 m by 15 m clipped square gridshell with a grid density of 20 and continuous bracing over half of the grid spaces is considered the best fit for the HA/DR scenario described throughout this paper. It is important to realize that the results are scalable in size, and that based on which characteristics are considered most important, there may be other gridshell designs well suited for HA/DR.

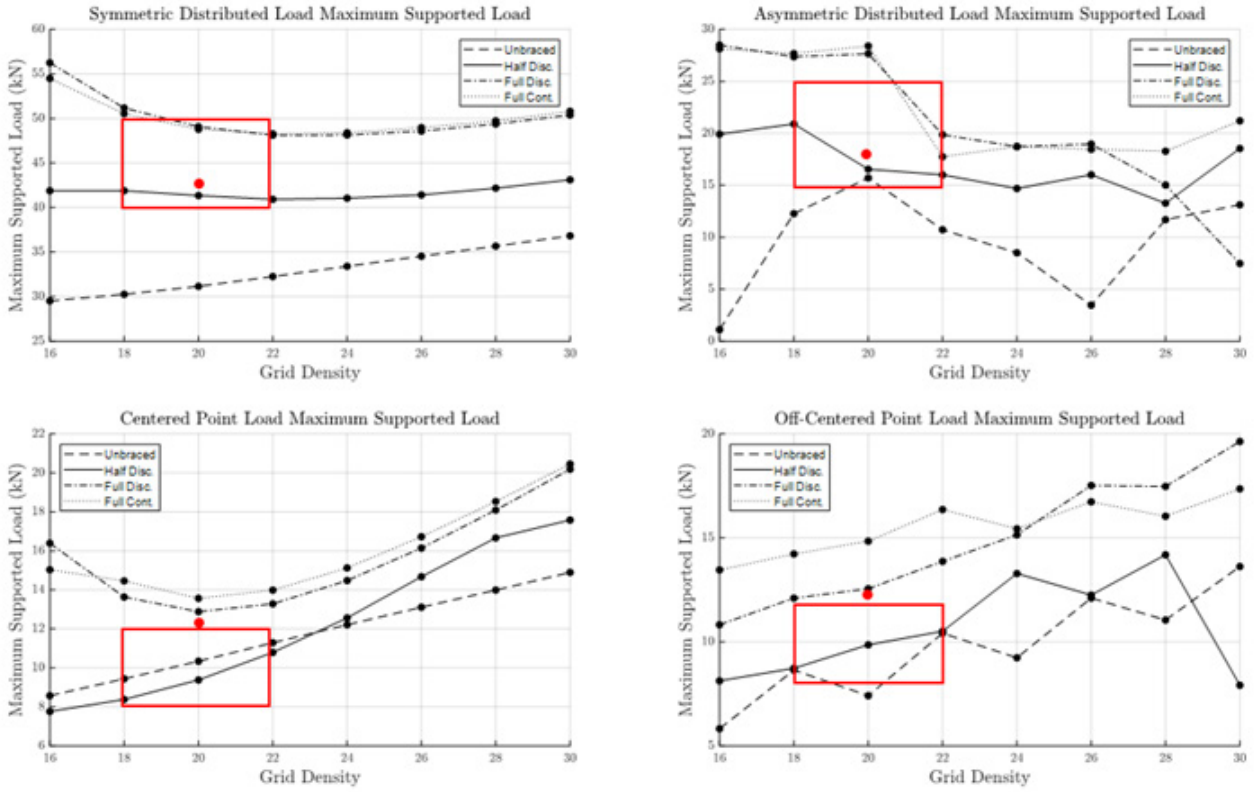

Figure 7: Summary of structural performance for each load case with the desired performance zones designated boxed and a "20 by 20", continuous half-braced gridshell indicated with a dot marker

It is worth noting that with 64 people spread evenly across the structure mentioned above (1.875 m spacing between individuals), each would need to apply only 160 N of force, equivalent to lifting a 17 kg weight, to raise the shell. Scaffolding will likely be necessary during the construction process to help maintain the form, but with only 17 kg of mass allocated to each person, construction without the use of cranes or heavy machinery would be possible (Naicu, Harris, & Williams 2014). Additional personnel would further reduce the force per individual.

When designing a gridshell, the choice of a bracing pattern and grid density is a combinatorial problem, which makes any optimization algorithm increasingly difficult to fashion. Instead, this paper suggests that given a general gridshell structure subjected to various load cases, bracing geometries, and grid densities, designers can choose from the results a performance region suited to their needs. By understanding the overall trends of the structures in questions, engineers can converge on solutions more quickly and can build a better understanding of how various parameters impact structural performance. Once a gridshell is selected, higher fidelity analysis that considers true single layer behaviour versus that of the continuous lattice assumption, joint stiffness, horizontal loading, and anchoring conditions must be completed.

6 CONCLUSION

Gridshells are designed to withstand many load cases, but regardless of the load case, the dominant failure mode is often global buckling. Proper bracing helps to stiffen and strengthen these structures in order to withstand symmetric and asymmetric distributed loads, as well as various point loads. Across each of the load cases studied in this paper, additional bracing has the greatest effect on improving load carrying capacity. Increasing the grid density is quite effective in improving the structure's resistance to failure under point loading. The continuity of the bracing shows little variation between fully-braced schemes, but continuous half-braced schemes consistently outperform discontinuous half-braced schemes. Using this data and methodology, designers can focus on structural characteristics based on the intended application of the shell. By selecting the structure that best fits the specified performance metrics, the data and methodology presented here can help designers select gridshells that are well suited for applications beyond their traditional niche. This paper makes the case that gridshell structures can be adapted to support large-span shelter needs in HA/DR scenarios.

Figure 8: (*left to right*) *Prototype of HA/DR gridshell – at the Harvard Humanitarian Initiative in* 2017 *and as a full-scale computer rendering*

7 FUTURE WORK

Research at the U.S. Naval Academy, coordinated by Professor Samar Malek over the past seven years, with the input of Professor Dave Polatty at the U.S. Naval War College, and numerous students, has already made strides to establish gridshell structures as potential solutions for large-span HA/DR shelters. Small-scale prototypes have featured at the Harvard Humanitarian Initiative, see Fig. 8, and continue to draw interest from the U.S. Naval War College Humanitarian Response Program. A large-scale prototype is ready for construction in the spring of 2021. Current research efforts have advanced the possibility of employing gridshell structures in HA/DR, yet additional work to investigate cladding, construction mechanics, and supply chains remains relevant.

With additional research and development, gridshell structures have the potential to serve in a variety of settings as a lightweight, natural, portable, adaptable, and efficient means for providing large-span shelter to remote regions. Gridshell technology can be refined and codified into design rules of thumb in order to lower the barrier to entry on these structures. By improving understanding and simplifying design approaches, these structures could serve to fill a much-needed role in HA/DR efforts and beyond as portable large-span structures.

8 ACKNOWLEDGEMENTS

This research would not have been possible without the Trident Scholar Program at the U.S. Naval Academy, the Office of Naval Research, Mr. Nick Hlavaty at the U.S. Naval Academy Technical Support Division, and Professor Dave Polatty at the U.S. Naval War College.

9 REFERENCES

Adriaenssens, S., Ney, L., Bodarwe, E., et al., (2009) Dutch Maritime Museum: Form-finding of an irregular faceted skeletal shell- Part b. In: A. Domingo and C. Lazaro, eds. *International Association for Shell and Spatial Structures Symposium,* Valencia, Spain. pp. 1356-1366.

Concrete Canvas Limited, (2018) *Concrete Canvas Shelters.* [Viewed 19 July 2019]. Available from: https://www.concretecanvas.com

Disaster Response in Asia and the Pacific (2013) *United Nations Office for the Coordination of Humanitarian Affairs* [online]. [Viewed 23 July 2019]. Available from: https://www.unocha.org/sites/unocha/files/dms/ROAP/Promotional%20Materials/The%20Guide-Web-FINAL.pdf

Edilsider SpA., (© 2020) *Edilsider*: *The Reference Point for Your Operational Needs.* [Viewed July 20 2019]. Available from: https://www.edilsider.com/edilsider-42.html

Figures at a Glance (2020) *United Nations Office for the Coordination of Humanitarian Affairs* [online]. [Viewed 25 July 2020]. Available from: https://www.unhcr.org/uk/figures-at-a-glance.html

Happold, E. & Liddell, W., (1975). Timber lattice roof for the Mannheim Bundesgartenschau. *The Structural Engineer*. 53, 99–135.

Knippers, J. & Helbig, T., (2009) *Recent Developments in the Design of Glazed Grid Shells. International Journal of Space Structures* [online]. 24, 111-126. [Viewed 20 February 2018]. Available from: doi: 10.1260/026635109789043205

Liddell, I., (2015) *Frei Otto and the Development of Gridshells. Case Studies in Structural. Engineering* [online]. 4, 39–49. [Viewed 19 July 2019]. Available from: doi: 10.1016/j.csse.2015.08.001.

Malek, S., Wierzbicki, T., & Ochsendorf, J., (2014) Buckling of spherical cap gridshells: A numerical and analytical

study revisiting the concept of the equivalent continuum. *Engineering Structures.* 75, 288–298.

McCormick, S., Besjak, C., Korista, S., et al., (2003) Shell of Steel. *Civil Engineering—ASCE.* 73, 68–73.

Naicu, D., Harris, R. & Williams, C., (2014) Timber Gridshells: Design methods and their application to a temporary pavilion. In: A. Salenikovich, ed. *World Conference on Timber Engineering,* Quebec City, Canada.

Operator's and Unit Maintenance Manual, Including Repair Parts and Special Tools List for Modular General Purpose Tent System (1999) Washington D.C.: Department of the Army.

Project for Public Spaces, (2018). *What can public spaces offer to the globally displaced?* [online]. Project for Public Spaces. [Viewed 16 July 2019]. Available from: https://www.pps.org/article/refugees-and-public-space.

Schlaich, M., Burkhardt, U., Irisarri, L., et al., (2009) Palacio de Comunicaciones- a single layer glass grid shell over the courtyard of the future town hall of Madrid. In: A. Domingo and C. Lazaro, eds. I*nternational Association for Shell and Spatial Structures Symposium*, Valencia, Spain. Madrid: International Association of Shell and Spatial Structures, pp. 1338-1348.

Sischka, J., (2000). Engineering the construction of the Great Court roof for the British Museum. In: M. Barnes, M. Dickson and T. Telford, eds. *Widespan Roof Structures.* London: ICE Publishing. pp. 199–207.

Determining Hydraulic Ram Pump Feasibility

Max Pawlick
Clemson Engineers for Developing Countries, Clemson University,
Clemson, South Carolina mpawlic@g.clemson.edu

David E. Vaughn
Clemson Engineers for Developing Countries, Clemson University,
Clemson, South Carolina
dev@clemson.edu

Jeffery M. Plumblee
Founder, Clemson Engineers for Developing Countries, Clemson University,
Clemson, South Carolina
jplumblee@gmail.com

ABSTRACT: *Hydraulic ram pumps have been used for over 200 years to pump water using only the potential energy of elevated water. Today, the low price and simplicity of the materials and methods required to construct ram pumps make them an excellent option for small and mid-sized water systems in developing countries where elevated water is available. However, ram pumps are risky to implement because they will fail to deliver water if they are not designed correctly. Currently, the evaluation of ram pump designs requires complex computer modeling typically unavailable in developing countries. Existing design documents for users without a specialization in fluid mechanics use vague rules of thumb to simplify the design process. Unfortunately, these rules cannot reliably predict whether a ram pump will deliver water in many cases. This study models the acceleration of fluid in the drive pipe and the intensity of the pressure spike to determine the feasibility of a wide variety of ram pump designs with a higher degree of certainty than previous rules of thumb. The model can be used in a Matlab program that determines if a design will function based on design parameters input by the user. The Matlab method was used along with conservative assumptions to provide design guidelines that can be easily applied for a range of pumping requirements. The model also highlights the importance of the fall to length ratio of the drive pipe, which can be leveraged to improve performance. These findings encourage a wider proliferation of hydraulic ram pumps through more accurate design tools and can reduce the cost of water systems for small developing communities.*

KEYWORDS: *hydraulic ram pumps, rural water systems, off-grid systems, hydraulic system modelling*

1 INTRODUCTION

1.1 Overview

Hydraulic ram pumps are devices capable of using the potential energy of elevated water to lift a fraction of that water to higher elevation. They are 'powered' by the water hammer effect that occurs when their waste valve slams shut due to the force of flowing water. Ram pumps are useful in rural or developing areas because they require no power source, no specialized training to maintain, and can be effectively built and repaired with basic construction methods and widely available pipe fittings. These characteristics are useful because reliable electrical grids, specialized parts, and skilled labor required by externally powered pumps are costly or unavailable in developing countries.

Unfortunately, ram pump systems are difficult to design because their operation and performance is highly dependent on numerous aspects of the site geography and pump design. Commonly used design methods are highly uncertain because they follow vague rules of thumb or use unreliable equations (Young 1997). Numerical analyses using a partial derivative formulation have successfully predicted performance characteristics for a small amount

of experimental data; however, the methods developed are difficult to implement for users without a high competency in numerical methods and programming (Filipan, Virag, & Bergant 2003). Several non-dimensional correlations for ram pump performance have been proposed based on experimental data (Fatahi-Alkouhi & Lashkarara 2017; Young 1997). However, these correlations cannot be used to determine the limitations of a design because they do not fully characterize the acceleration of flow in the drive pipe.

The service-learning organization Clemson Engineers for Developing Countries has cancelled multiple ram pumps projects because the site conditions are not robust enough to guarantee a ram pump will function. This uncertainty has likely led to the underuse of ram pumps by humanitarian organizations and developing communities themselves, as both groups are unlikely to invest in water projects that may not deliver sufficient or any water.

This investigation models the ram pump operating cycle with basic fluid mechanics principles to develop a Matlab based method for evaluating ram pump designs. The method provides the design boundaries of feasible ram pump systems with less uncertainty than current design methods. The user does not require any technical background to evaluate the design and can analyze a wide array of possible designs due to the fundamental nature of the model. The Matlab script was used to produce a reference table that provides the minimum site requirements for a pump to be feasible across several common scenarios. Users without access to Matlab can also solve the nonlinear differential equations in the model with a simple Euler approach using a spreadsheet software. The investigation also indicates the importance of the fall height to drive pipe length ratio, which has been absent from previous non-dimensional analyses.

1.2 Definition of Terms

- Fall Height - Elevation change from the top of the water source to the waste valve (or water line above the waste valve if it is submerged.)
- Lift Height - Elevation change from the internal check valve of the pump to the location water will be delivered.
- Fall to Length Ratio - Equal to the fall height divided by the drive pipe length.
- Spike Velocity - The average velocity of the water in the drive pipe at the instant the waste valve slams shut.
- Spike Pressure - The peak pressure created each time the waste valve slams shut.

1.3 Definition of Mathematical Symbols

- h_f – fall height (supply head)
- h_l – lift height (delivery head)
- $h_{l\,max}$ – maximum lift height of a pump
- F – force on the waste valve wafer due to the waste flow
- F_a – gravitational force accelerating the drive pipe flow
- F_p – frictional force on the drive pipe flow from the drive pipe wall
- F_m – force acting on the drive pipe flow due to minor losses throughout the drive pipe
- f_d – Darcy friction factor
- m – mass of water in the drive pipe
- r – inner radius of the drive pipe
- r_w – radius of the waste valve wafer
- V – flow velocity
- V_s – spike velocity
- P_s – spike pressure
- P_{loss} – instantaneous pressure loss per unit length in the drive pipe
- t_s – acceleration time required to reach spike velocity
- x – distance traveled by the flow
- x_s – distance flow must advance each pump cycle to reach the spike velocity
- C_w – wave velocity in the drive pipe
- B – bulk modulus of water
- K – Minor loss coefficient
- E – Young's modulus of the drive pipe material
- e – wall thickness of the drive pipe
- D – inner diameter of the drive pipe
- A_c – cross sectional area of the drive pipe
- l – drive pipe length
- T_w – pipe wall shear stress
- ϵ – absolute roughness of the drive pipe
- Re – Reynold's number
- μ – dynamic viscosity of water
- ν – kinematic viscosity of water
- Q_s – flowrate supplied to pump
- Q_d – flowrate delivered by the pump
- Q_w – waste flow rate of pump
- Q_c – instantaneous waste flowrate immediately preceding the pressure spike
- ρ – density (water)

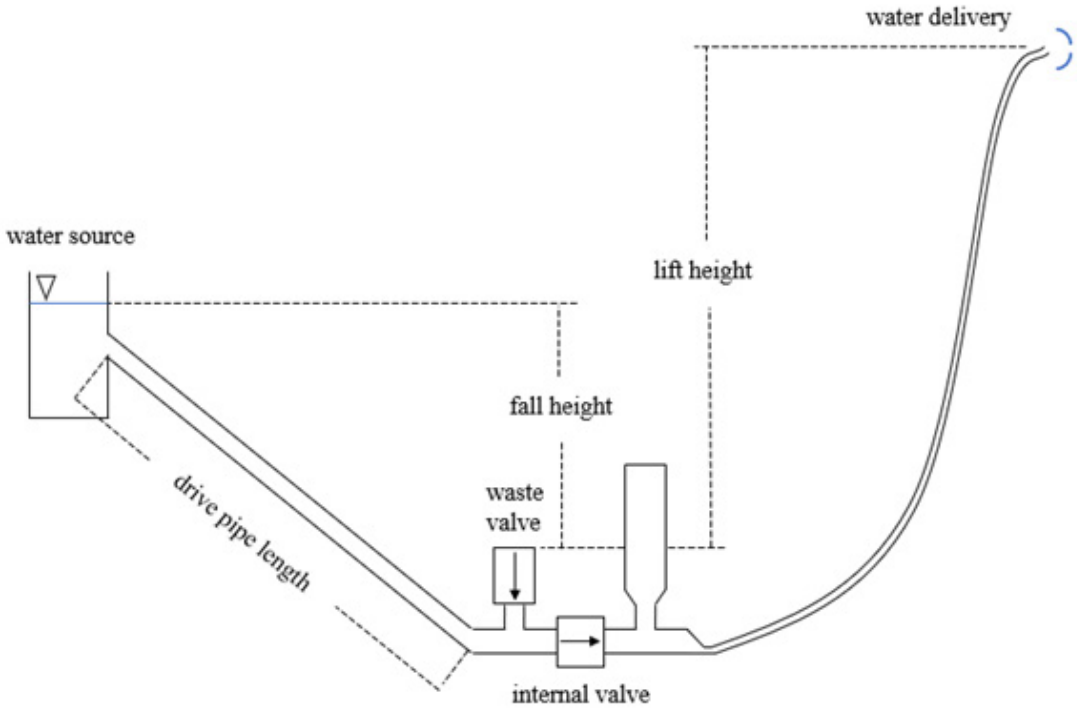

Figure 1: *Ram pump system schematic*

1.4 Ram pump setup and cycle

The typical ram pump installation is illustrated in Figure 1.

The ram pump uses the elevated water source to initiate flow through its drive pipe and waste valve (typically a check valve). The flow accelerates due to the gravitational potential energy of the fall height at a rate determined by the fall to length ratio until the force of the water moving though the waste valve slams it shut. At this point, the water stops suddenly, leading to a pressure spike due to the water hammer effect. This pressure opens the internal valve (also a check valve) and moves a small amount of water through it against the head pressure of the lift height. Concurrently, the pressure spike sends a pressure wave up the drive pipe to the free surface of the water source. Once the wave reaches the free surface, a low-pressure wave propagates back down the drive pipe until it reaches the internal valve. This causes the internal valve to close due to the lift height pressure, and the waste valve to open. Water begins to accelerate out of the waste valve again and the cycle repeats indefinitely (Glover 1994).

1.5 Current design methods

Currently, most ram pump systems are designed by assuming a certain input flowrate and an efficiency of 60% (Rife Hydraulic Engine Manufacturing Co 1985; Smith 2017). These two parameters can be used along with the lift height and fall height to calculate the delivery flowrate using the definition of pump efficiency given in equation 1.

$$\eta = \frac{Q_d h_l}{Q_s h_f} \tag{1}$$

Arbitrarily assuming an efficiency of 60% is problematic because real efficiencies can range from at least 0 to 65% and vary as a function of as many as 11 independent variables (Fatahi-Alkouhi & Lashkarara 2017). Most importantly, this design method leaves users to guess the input flowrate and fall height their pump will require across wide experimental ranges. This guess is critical because the pump will fail if the water source flowrate or fall height is not sufficient to generate a spike pressure capable of opening the internal check valve. This method ignores the impact of low fall to length ratios, which can also cause the pump to fail due to insufficient acceleration of the drive pipe flow.

Other methods use experimental data and dimensionless groups to predict performance criteria. However, these methods do not consider cases where maximum velocity or input flowrate of the water is insufficient for certain lift heights (Fatahi-Alkouhi & Lashkarara 2017; Young 1997). As a result, they cannot be used to reliably determine the feasibility of a design.

2 METHODOLOGY

A model was developed to predict the fall height, fall to length ratio, and drive pipe flowrate required to achieve a certain spike pressure. The model can be applied to any ram pump design with a single waste valve.

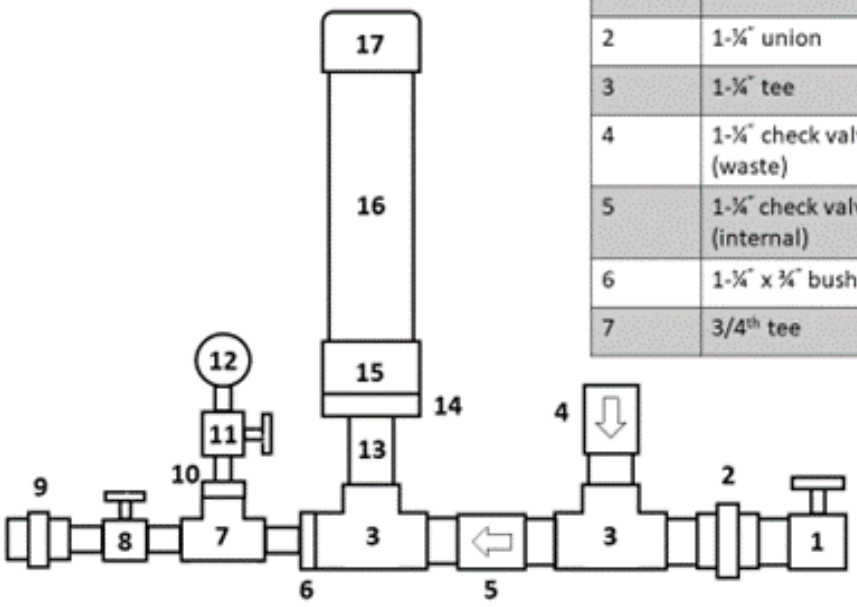

Number	Item	Number	Item
1	1-¼" valve	8	¾" valve
2	1-¼" union	9	¾" union
3	1-¼" tee	10	¾" to ¼" bushing
4	1-¼" check valve (waste)	11	¼" inch valve
5	1-¼" check valve (internal)	12	100 psi pressure gauge
6	1-¼" x ¾" bushing	13	1-¼" nipple
7	3/4th tee	14	4" to 1-¼" bushing
		15	4" coupling
		16	4" by 24" pipe (rated > 160 psi)
		17	4" PVC Glue Cap
			Inner tube (not shown)

Figure 2: Mark Risse ram pump design

A ram pump was constructed from PVC pipe and fittings to conduct experiments from a design by Mark Risse (Smith 2017). A schematic of the design is shown in Figure 2.

The design features a drive pipe with an inner diameter of 34.5 mm and a wall thickness of 7.6 mm. Experiments were conducted using both a brass swing check and weighted poppet-style brass spring check valves for the pump's waste valve, which is shown as item 4 in Figure 2. A PVC poppet-style spring check valve was used for the internal valve which is shown as item 5 in Figure 2. The same nominal size as the drive pipe was used for the internal valve and waste valves. The pump used for testing is shown in the image below, where a wire wheel brush is attached to the waste valve wafter to increase its weight.

Increased lift heights were simulated by partially closing a globe valve on the end of the delivery line. The maximum lift height, corresponding to an efficiency of zero, was measured by closing the globe valve completely. The experimental lift height was determined by reading a pressure gauge at the bottom of the delivery line and translating it to a pressure head. This method allowed experiments to be run with delivery heads as high as 38.7 meters.

The ram pump was tested under five different cases with unique combinations of fall height, waste valve weight, and drive pipe length. For each case where the water velocity was sufficient to close the waste valve, the ram pump was tested at multiple simulated lift heights. The input and output flowrate were measured for each lift height by recording the time required to fill a container of known volume. The parameters of each test case are shown in Table 1.

Figure 3: The operating test ram pump

Table 1: *Experimental test cases*

Case Number	Fall Height [m]	Valve Weight [kg]	Drive Pipe Length [m]	Maximum Lift Height [m]
1	3.58	0.153	14.72	33.8
2	3.58	0.286	14.72	49.3
3	3.58	Swing Check	14.72	42.3
4	1.83	Swing Check	11.06	42.3
5	1.83	0.286	11.06	0

For the fifth case, the maximum water velocity at the waste valve was not enough to close the waste valve regardless of input flowrate. As a result, no water could be delivered regardless of simulated lift height. The pump efficiency for each test was calculated according to Equation 1 by using the simulated lift height, the fall height, and the measured input and output flowrates. These results are shown in Figure 4.

The range of efficiencies reported is between 0 and 57%. The results indicate the efficiency is dependent on several variables including the fall height, lift height, and waste valve properties. The maximum lift height for cases 1-4 along with the complete failure of the pump in case 5 highlight the possibility for ram pumps to fail to deliver water after installation.

The operation of a generalized ram pump was modeled to provide a conservative estimate of the maximum lift height that can be achieved assuming the user can modify the weight of a circular waste valve wafer.

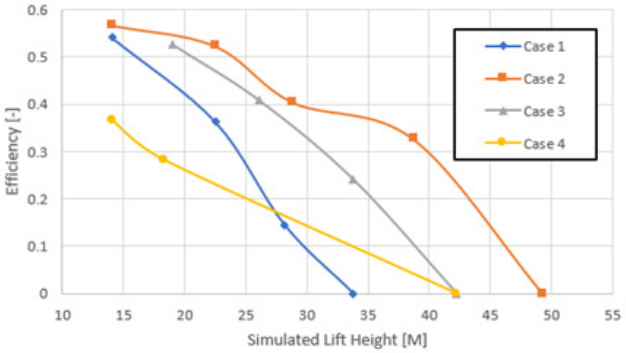

Figure 4: *Experimental ram pump efficiencies*

3 EVALUATION

3.1 Estimating spike pressure

To ensure the drive pipe has enough length to fully develop the pressure spike, the drive pipe length should be sized between 150 and 1000 times the diameter of the pipe (Calvert 1958). In a pump with a properly sized drive pipe, the spike pressure reaches its maximum intensity, which can be calculated from Equation 2 (Joukowsky 1904).

$$P_s = V_s \rho C_w \tag{2}$$

where the wave velocity, C_w, can be calculated with Equation 3.

$$C_w = \sqrt{\frac{1}{\rho\left[\frac{1}{B}+\frac{D}{Ee}\right]}} \tag{3}$$

To determine how accurate the application of this equation was to experimental ram pumps, three tests were conducted to measure the pressure spike with known waste valve wafer masses. For each test, a theoretical spike velocity was calculated based on the mass of the waste valve wafer. This velocity was used to calculate the theoretical pressure spike. The experimental pressure spike was measured by closing the valve on the pump delivery line to simulate the pump operating at maximum lift height (with no delivery flow). The pressure was read from a standard gauge at the bottom of the delivery line between spikes.

An equation describing the water velocity needed to overcome the mass of the valve wafer was needed to complete this analysis. Since the waste valve closure must be rapid for the pump to function properly, the valve was modelled to close immediately once the gravitational force of its wafer mass was exceeded. The force of the flow on the stationary valve wafer is between that of a jet and a disk experiencing drag in an external flow because there is a limited amount of free area around the valve wafer. Modelling the flow's force as that of a jet was found to predict the spike pressure more accurately than using the drag force equation. For waste valves with a circular wafer the force due to a jet reduces to Equation 4.

Table 2: Calculated and measured spike pressures

Mass [grams]	Theoretical velocity [m/s]	Theoretical spike [kPa]	Experimental spike [kPa]	Ratio [-]
153	1.06	399	345	0.863
286	1.45	547	483	0.883
211	1.24	470	421	0.896

$$F = \rho(\pi {r_w}^2){V_s}^2 \quad (4)$$

The force analysis for swing check valves is more involved because the orientation of the wafer is not perpendicular to the waste flow. It was experimentally determined that the spike velocity for a 1 ¼ inch brass swing check valve oriented vertically was approximately 1.22 m/s. This result was similar to the 1.34 m/s close velocity listed in friction loss tables (PlumbingSupply.com 1995). The spike velocity of a swing check valve is a function of the mass per unit area of the wafer and its angle relative to the flow path. Since these properties change little between valve sizes, approximations of the spike velocity between 1.22 and 1.34 m/s are assumed valid for brass swing check valves of other sizes.

The data from these experiments is shown in the table below, where the theoretical velocity is calculated by solving Equation 4 for spike velocity.

From the experiments, it appears the spike pressure is between 85 and 90% of the theoretical spike pressure. Based on this observation, the model uses Equation 2 and multiplies the product by 0.8 to calculate the spike pressure of a pump. This factor adjusts the calculation to account for the experimental differences and provides a small safety factor. The spike pressure can be divided by the water density and acceleration due to gravity to calculate the maximum lift height of the pump. Accurately predicting the spike velocity is important to predict the waste valve weight and the amount of inflow the pump requires.

3.2 Acceleration of drive pipe flow

The acceleration of flow in the drive pipe must be modelled to predict the amount of water required to complete a pump cycle, the pump's frequency, and the maximum spike velocity attainable. These quantities are used to calculate the lift heights a pump can achieve, and the corresponding supply flowrates required.

Each time a ram pump cycles, the water in the drive pipe begins at a negative velocity from the recoil of the previous cycle (Glover 1994). This negative velocity is generally small in comparison to the spike velocity. The model assumes the flow is stationary at the beginning of each cycle, which simplifies the analysis while yielding an upper bound for the required inflow. If the pump is designed correctly, gravity causes the flow to accelerate until the flow reaches the spike velocity required to close the waste valve. However, if the fall height, or fall to length ratio is insufficient, the flow will stop accelerating before the waste valve closes and the pump will not operate.

The fluid inside the drive pipe is analyzed as a control volume, and the acceleration of the flow is modelled as one-dimensional incompressible flow. These assumptions eliminate relative motion in the fluid, allowing for an analysis based on rigid body translation (Munson, Okiishi & Huebsch 2009). When analyzed as a rigid body, the control volume acceleration can be described by Newton's second law as shown in Equation 5,

$$m\frac{dV}{dt} = F_a - F_p - F_m \quad (5)$$

where m is the mass of the accelerated water in the drive pipe, F_a is the acceleration force due to gravity, F_p is the force associated with pipe friction, and F_m is the force associated with minor losses including the waste valve and any other flow restrictions.

The total acceleration force acting on the control volume is the product of the total hydrostatic pressure available, and the cross-sectional area of the pipe as given in Equation 6.

$$F_a = \rho g h_f A_c \quad (6)$$

The pipe friction force can be expressed as the product of the wall shear stress and the total pipe surface area as given in Equation 7.

$$F_p = T_w \pi D l \quad (7)$$

The shear stress on the pipe wall can be modelled with the same methods used to predict pressure drop in pressurized systems. Pressure drop per unit length is related to the wall shear stress by Equation 8 (Munson, Okiishi & Huebsch 2009).

$$\frac{dp}{dl} = \frac{2\tau_w}{r} \quad (8)$$

The Darcy-Weisbach equation was used to model pressure drop. It is given in Equation 9,

$$\frac{dp}{dl} = f_d \frac{\rho V^2}{2D_h} \tag{9}$$

where f_d is the Darcy friction factor. While the flow is laminar $f_d = 64/Re$. In this case the pipe friction force is given by Equation 10.

$$F_p = 8\pi l V \mu \tag{10}$$

For most ram pump applications, the drive pipe flow becomes turbulent soon after acceleration begins. For turbulent flow, f_d can be approximated explicitly by Equation 11 (Swamee and Jain 1976).

$$f_d = \frac{0.25}{\left(log_{10}\left(\frac{\epsilon}{3.7D}+5.74\left(\frac{\nu}{VD}\right)^{0.9}\right)\right)^2} \tag{11}$$

Rewriting Equation 7 using Equations 9 and 11, yields an expression for pipe friction force when the flow is turbulent in terms of physical constants and velocity. This expression is given in Equation 12.

$$F_p = \frac{\rho V^2 \pi D l}{32\left(log_{10}\left(\frac{\epsilon}{3.7D}+5.74\left(\frac{\nu}{VD}\right)^{0.9}\right)\right)^2} \tag{12}$$

The force associated with minor losses is modeled with the excess head method. The excess head method assumes the pressure loss across an obstruction is proportional to the square of the velocity. The loss coefficient, or proportionality constant, K, of various bends, valves, and fittings can be found in a wide range of reference materials (Munson, Okiishi & Huebsch 2009). A loss coefficient may also be used to account for the presence of a course filter at the drive pipe inlet if one is used. The force due to minor losses can be expressed as the summation of all the minor losses that would be expected in a pressurized system multiplied by the cross-sectional area of the drive pipe. It is assumed here that any obstructions causing minor losses have the same nominal diameter, and therefore the same one-dimensional velocity, as the drive pipe. This assumption yields Equation 13.

$$F_m = \sum K \rho \frac{V^2}{2} A_c \tag{13}$$

The rigid body acceleration described in Equation 5 can now be written for the general case as shown in equation 14.

$$m\frac{dV}{dt} = \rho g h_f A_c - \frac{1}{8}\pi D l \rho V^2 f_d - \sum K \rho \frac{V^2}{2} A_c \tag{14}$$

The equation can be simplified by replacing m with the product of fluid density and drive pipe volume, and solving for the acceleration term. The result for the laminar case is shown in Equation 15.

$$\frac{dV}{dt} = g\frac{h_f}{l} - 32\frac{\nu V}{D^2} - \frac{\sum K V^2}{2l} \tag{15}$$

The result for the turbulent case is shown in Equation 16.

$$\frac{dV}{dt} = g\frac{h_f}{l} - \frac{V^2}{8D\left(log_{10}\left(\frac{\epsilon}{3.7D}+5.74\left(\frac{\nu}{VD}\right)^{0.9}\right)\right)^2} - \frac{\sum K V^2}{2l} \tag{16}$$

Equations 15 and 16 indicate the flow will stop accelerating (i.e., dV/dt = 0) at a velocity determined by the fall to length ratio, the characteristics of the drive pipe, and the total loss coefficient of the system. This implies that for a system where the effective weight of the waste valve can be adjusted, the fall to length ratio limits the spike velocity even for designs with large fall heights. This insight is largely absent in the literature.

3.3 Direct applications of the acceleration model

Matlab's 'ode45' a fifth order Runge Kutta ordinary differential equation solver is used to solve equation 14 for V(t) and its integral x(t) where the initial value of both variables is equal to zero. The equation can also be solved using a simple Euler technique in a spreadsheet software. The solutions can be used to estimate how much time, t_s, it takes the water to reach a certain spike velocity, V_s. This time can be used to calculate the maximum number of times a pump can cycle each minute. The solutions can also be used to calculate x_s, which represents the distance the flow must advance during each cycle and can be multiplied by the area of the drive pipe to obtain the waste flow volume required for each cycle.

To predict the maximum waste flowrate for design purposes, the negative velocity in the drive pipe after each cycle was neglected. The maximum frequency can be calculated by accounting for the time it takes for the flow to reach the spike velocity, and the time it takes the pressure wave to travel up and down the drive pipe. The maximum frequency can be found from Equation 17.

$$f = \frac{1}{t_s + \frac{2l}{c_w}} \tag{17}$$

Frequencies measured during testing were compared to the maximum frequency predicted by the model. The comparison is shown in Figure 5 where the frequency is displayed in cycles per minute.

The actual frequency of the pump during experimentation was found to be between 60% and 90% of the maximum value. This percentage is influenced by the recoil velocity magnitude, which is influenced by the lift height, fall height, pressure spike, and fall to length ratio of the system. The maximum waste flowrate required for the pump can be calculated by taking the product of the maximum frequency, the cross-sectional area of the drive pipe, and the distance the flow must advance for each cycle, x_s.

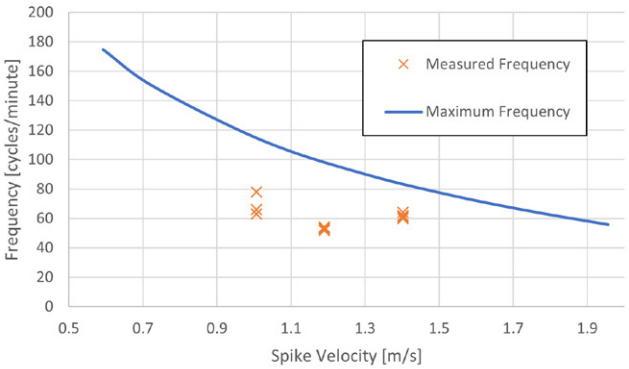

Figure 5: *Experimental and modelled maximum frequency*

To determine the maximum input flowrate required, the delivery flowrate must be known or assumed. The delivery flowrate can be expressed by rearranging Equation 1 as shown in Equation 18.

$$Q_d = \frac{\eta h_l Q_w}{(h_l + \eta h_f)} \tag{18}$$

Setting η equal to unity provides the maximum possible delivery flowrate, which can be added to the maximum possible waste flowrate to determine the maximum input flowrate required. It should be noted that the actual delivery flowrate cannot be calculated by the model, since no attempt was made to model the real efficiency.

The model was run over the same conditions as the experiments. The amount of waste water required for the experiments was compared to the maximum amount of waste water the model predicted. This comparison is displayed in the Figure 6.

The comparison indicates that the model is reasonably accurate. This uncertainty can be mitigated by using a small safety factor for the flowrate. The safety factor should also account for seasonal changes in the supply flowrate.

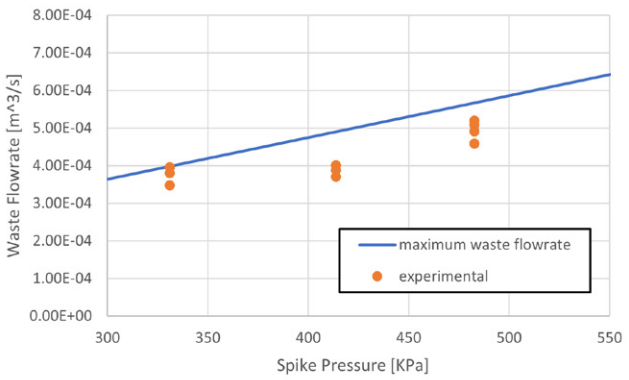

Figure 6: *Experimental comparison of waste water flowrate*

Designers can use the projected maximum flowrate to determine if their water source has a sufficient flowrate.

3.4 Estimating minimum fall height required

The maximum spike velocity of a ram pump can also be limited by the available fall height. To determine the amount of fall height required for a certain spike velocity, conservation of energy was applied to the flow in the drive pipe using Bernoulli's equation. As the flow in the drive pipe accelerates, the gravitational potential energy of the water is lost to kinetic energy and friction. The pressure loss that occurs during the acceleration of the flow to the spike velocity depends on the behavior of the velocity and the distance the flow translates during a cycle. The amount of gravitational potential energy per unit volume required to close the waste valve is shown in Equation 19 where V is a function of time which can be calculated from integrating Equation 14.

$$\rho g h_f = \frac{1}{2}\rho V(t)^2 + \int_0^{x_s} P_{loss}\big(V(t)\big)dx \tag{19}$$

The function P_{loss} is the pressure drop per unit length of the drive pipe, which includes the pressure loss due to pipe friction (major loss) and waste valve friction (minor loss). P_{loss} can be calculated with Equation 20.

$$P_{loss} = \frac{1}{2l} K \rho V(t)^2 + f_d \frac{\rho V(t)^2}{2D_h} \tag{20}$$

The integral in Equation 19 is calculated according to the trapezoidal rule, where an average value of P_{loss} during a time interval is determined from the numerical solution for $V(t)$. This value is then multiplied by the change in $x(t)$ over the time interval which can be obtained by integrating Equation 14 twice. These pressure drops are continually summed until $x(t)$ reaches x_s at which point the integration is complete.

Before the waste valve reopens to begin the next cycle, the low-pressure wave from the water source has propagated back down the drive pipe. Since this occurs very quickly in comparison to the acceleration of the flow, the drive pipe flow will begin accelerating with all of the potential energy of the fall height. This implies that the friction head loss does not accumulate each cycle.

This model is implemented in the Matlab script in the appendix. The script can be used to estimate the maximum spike pressure a pump can achieve as a function of drive pipe (length, diameter, material, wall thickness, average angle, bends), fall height, and the available supply flowrate.

4 DELIVERY FLOW OBSERVATIONS

Existing models of the delivery flowrate were compared against the experimental data obtained in this study to determine how accurately they predicted delivery flow for the experimental design. The first model is from Young (1997) and uses the peak instantaneous waste flowrate, Q c , as shown in Equation 21 to directly predict delivery flow.

$$\frac{Q_d h_l}{Q_c h_f} = 0.27 \pm 0.05 \tag{21}$$

When the results of this model were compared to experimental data, the model was found to be inaccurate as the ratio of lift height to fall height increased. The percent error of the experimental data is plotted in the Figure 7 with the lift to fall height ratio on the x-axis.

The figure indicates this model significantly underpredicts delivery flow as the lift to fall height ratio increases.

The data were also compared with an efficiency equation of a Jundi-Shapur University of Technology study derived from experimental results. The relationship is shown in Equation 22 (Fatahi-Alkouhi & Lashkarara 2017).

$$\eta = -0.2688 + \left(\frac{l}{D}\right)^{-0.0479} - 0.4763\left(\frac{h_l}{h_{lmax}}\right)^{1.2507} \tag{22}$$

This equation was found to predict pump efficiency accurately for the tests with a fall to lift ratio of 0.17. However, the model underpredicted the efficiency for tests with a fall to length ratio of 0.24. The comparison is shown in Figure 8.

The comparison indicates the model predicted only a slight difference in efficiency for the change in l/D, while the experimental data indicates a much larger difference. This is likely because the model does not directly account for the influence of the fall to length ratio. A steeper fall to length ratio will likely decrease recoil velocity because there is more resistance to backwards flow. This results in more of the pressurized flow being delivered during each pressure spike which raises pump efficiency. Additionally, the analysis in Section 3 shows higher fall to length ratios will increase the acceleration of the flow, leading to a lower waste flowrate and higher efficiency.

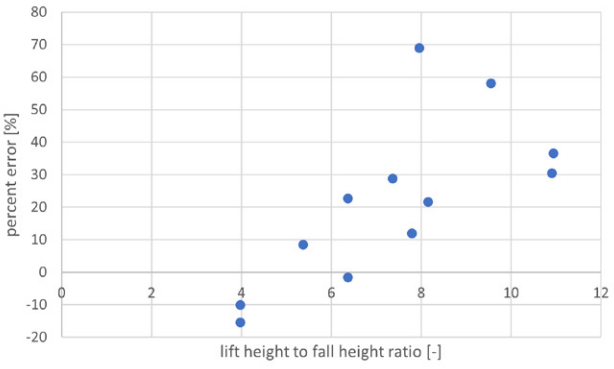

Figure 7: Experimental error in comparison to Young's model

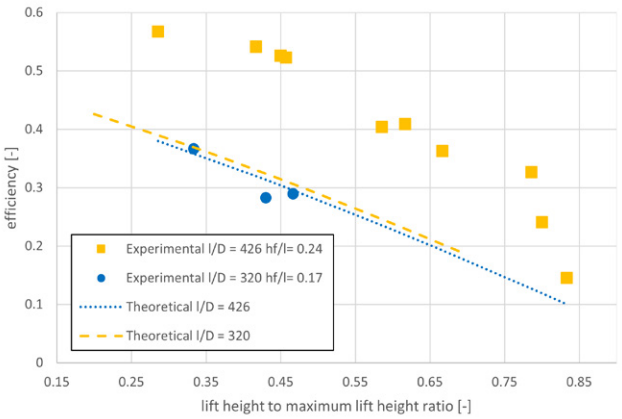

Figure 8: Experimental comparison of efficiency to Jundi-Shapur University model

Since existing correlations could not predict the delivery flow of this design reliably, the model developed in this paper does not predict the delivery flow of potential designs.

5 PRODUCING REFERENCE TABLES FROM MODEL

The acceleration model was conservatively applied to several example scenarios to determine the minimum site characteristics required to pump water for ram pumps with waste valve weights that can be adjusted. In this application it is assumed a site must produce a spike pressure 1.3 times greater than the lift height pressure to be considered feasible. This ratio was chosen based on experimental results that show delivery flow decreases sharply after this ratio. The ratio is similar to the 1.67 ratio recommended by Young (1997) when it is divided by the 0.8 factor used to determine the difference between theoretical and experimental pressure spike (Young 1997). These solutions also assume the drive pipe contains no tight bends, a spring check valve is used for the waste valve (with an assumed loss coefficient of 10), and the l/D ratio is at least 300. Systems that do not meet these criteria need to be evaluated with the Matlab script in the appendix or other numerical methods. To simplify the use of the figure, the results are displayed in both Metric and English units.

Figures 9 and 10 list the minimum site characteristics required to deliver water to different ranges of lift height using Metric and English units respectively. To evaluate a site, one should start by the finding the applicable lift height range. Then, compare the site's attributes with the minimum fall to length ratio (h_f/l), fall height (h_f), and

supply flowrate (Q_s) required for the types of drive pipes being considered for the design. If the site meets or exceeds all three of these requirements, a ram pump is feasible for the relevant drive pipe type. For some cases the angle and fall height boxes contain two values separated by a '|' symbol. In these cases, there are two sperate minimums for the fall to length ratio and fall height. For example, Figure 9 indicates a pump with a 26 mm inner diameter and 3.4 mm wall thickness made of PVC with a lift height between 30 and 46 meters and a fall to length ratio of 0.17 would require 6.71 meters of fall height, but if the pump had a fall to length ratio of 0.26, only 4.27 meters of fall height would be required. If the site exceeds some requirements but falls short in others the design needs to be studied using the Matlab script (included in the appendix) to determine feasibility.

As any pump approaches the minimum requirements for its lift height, the efficiency and therefore the flow rate it will deliver decreases exponentially as shown in Figure 8. The delivery flow of a system will largely depend on the system's drive pipe (diameter, length, and average angle) and fall height. Sites that require low values for those characteristics, such as steel pipes for low delivery heights, will deliver a smaller fraction of their inflow. The arrangement of the site should seek to exceed the minimum requirements to deliver more water. Stand pipe systems can often be used to increase the fall to length ratio if necessary (Rife Hydraulic Engine Manufacturing Co 1985).

For a design with an adjustable waste valve to operate correctly, its valve wafer must have the correct amount of weight to prevent the valve from closing until the flow reaches the desired spike velocity. Weight can be added to most spring check valves by disassembling them and attaching mass to the stem before reassembly. If the site characteristics surpass the minimum requirements, more mass can be added to the waste valve wafer to deliver more water. However, adding additional mass will raise the amount of supply flow required, and may raise the fall height, and average drive pipe angle required. The weight required for the maximum spike velocity can also be estimated with the Matlab script or with Equation 4. Figures 11 and 12 list the aggregate mass of the wafer and additional weight in required in grams and ounces respectively for the same scenarios listed in Figures 9 and 10.

6 CONCLUSION

The methods presented allow for the feasibility of a hydraulic ram pump project to be determined by a user without specialized skills with more accuracy than was previously possible. The characterization of the drive pipe acceleration and pressure spike allows users to predict the maximum lift height of most ram pump designs more accurately than previous design methods. While ram pumps will deliver water to lift heights below their maximum, comparisons with experimental data indicated current

	Pipe Material	PVC			Steel		
	Inner Diameter [mm]	26	52	77	26	52	77
	Wall Thickness [mm]	3.4	3.9	5.5	3.4	3.9	5.5
Lift Height [m]		Requirements					
23-30	hf/l [-]	0.13	0.09|0.13	0.09|0.13	0.05	0.05	0.05
	hf [m]	2.14	4.27 | 2.74	3.96 | 2.44	1.52	0.92	0.92
	Q [l/min]	19.0	71.9	140.0	11.4	34.1	72.0
30-46	hf/l [-]	0.17|0.26	0.26	0.17|0.26	0.09|0.13	0.09	0.05|0.09
	hf [m]	6.71 | 4.27	7.01	11.28 | 6.10	2.44 | 1.22	1.53	3.05 | 1.22
	Q [l/min]	26.5	102.2	234.7	15.1	49.2	113.6
46-61	hf/l [-]	0.34	0.26	0.26	0.13|0.17	0.09|0.12	0.09|0.13
	hf [m]	7.62	11.59	10.67	4.57 | 3.05	3.96 | 2.44	3.35 | 1.83
	Q [l/min]	32.2	257.4	265.0	22.7	72.0	143.8
61-76	hf/l [-]	0.50	X	X	0.26	0.13|0.17	0.13|0.17
	hf [m]	12.20	X	X	4.57	4.88 | 3.66	4.88 | 3.05
	Q [l/min]	37.9	X	X	26.5	87.1	181.7
May require thicker piping to handle pressure			Not Feasible				

Figure 9: Minimum site characteristics required for various ram pump configurations in Metric units

		PVC Schedule 40			Steel Schedule 40		
Lift Height [ft]	Requirements	1 in	2 in	3 in	1 in	2 in	3 in
75-100	hf/l [-]	0.13	0.09|0.13	0.09|0.13	0.05	0.05	0.05
	hf [ft]	7	14 | 9	13 | 8	5	3	3
	Q [gal/min]	5	19	37	3	9	19
100-150	hf/l [-]	0.17|0.26	15	0.17|0.26	0.09|0.13	0.09	0.05|0.09
	Hf [ft]	22 | 14	23	37 | 20	8 | 4	5	10 | 4
	Q [gal/min]	7	27	62	4	13	30
150-200	hf/l [-]	0.34	0.26	0.26	0.13|0.17	0.09|0.12	0.09|0.13
	hf [ft]	25	38	35	15 | 10	13 | 8	11 | 6
	Q [gal/min]	8.5	68	70	6	19	38
200-250	hf/l [-]	0.50	X	X	0.26	0.13|0.17	0.13|0.17
	hf [ft]	40	X	X	15	16 | 12	16 | 10
	Q [gal/min]	10	X	X	7	23	48
May require Schedule 80 piping to handle pressure			Not Feasible				

Figure 10: *Minimum site characteristics required for various ram pump configurations in English units*

Pipe Material	PVC			Steel		
Inner Diameter [mm]	26	52	77	26	52	77
Wall Thickness [mm]	3.4	3.9	5.5	3.4	3.9	5.5
Lift Height [m]	Waste valve weight [g]					
23-30	110	600	1350	32	130	292
30-46	220	1600	3750	73	292	658
46-61	375	2500	5200	135	520	1170
61-76	600	X	X	203	812	1827

Figure 11: *Minimum mass of waste valve wafer required in metric units (grams)*

Lift Height [ft]	PVC Schedule 40			Steel Schedule 40		
	1 in	2 in	3 in	1 in	2 in	3 in
	Waste valve weight [oz]					
75-100	4	21	48	1	5	10
100-150	8	56	132	3	10	23
150-200	13	88	183	5	18	41
200-250	21	X	X	7	29	64

Figure 12: *Minimum mass of waste valve wafer required in English units (ounces)*

models for predicting delivery flow are inaccurate in some cases.

Users can make more informed project decisions by using the provided reference scenarios or evaluating specific designs in the numerical model. This information makes ram pump projects less risky investments for those working in developing communities and should lead to a wider proliferation of ram pumps. The model can be used by those designing or troubleshooting ram pump systems to better understand how different variables effect pump performance. The model also highlights the importance of the fall to length ratio for pump feasibility and efficiency.

While the experimental data supported the findings of the model, the data were only recorded over a limited range of design scenarios. Further testing should be conducted across pumps with various design characteristics to evaluate the accuracy of the model across a wider range of scenarios. Additionally, more research is needed to accurately predict the amount of water a pump can deliver each cycle. A dimensional analysis that includes the fall to length ratio as a parameter is a good candidate. Accurately predicting the amount of delivery flow would allow larger ram pump systems to be designed and implemented with a high degree of confidence, which would likely increase the affordability and reliability of water supply systems in the developing world.

7 REFERENCES

Calvert, N. (1958) 'Drive pipe of a hydraulic ram', *The Engineer,* Harmsworth Press, London, England, 26 December, 206 (5370), p. 1001

Fatahi-Alkouhi, Reza & Lashkarara, Babak. (2017) 'Experimental evaluation of effective parameters on characteristic curves of hydraulic ram-pumps' *Scientia Iranica*. 26. 10.24200/sci.2017.4597.

Filipan, V., Virag, Z. & Bergant, A. (2003) 'Mathematical modelling of a hydraulic ram pump system' *Journal of Mechanical Engineering* 49(3):137-149

'Friction Loss Tables', (1995) PlumbingSupply.com. https://www.plumbingsupply.com/ed-frictionlosses.html, Accessed 6 November, 2022

Glover, Peter B.M. (1994) '*Computer simulation and analysis methods in the development of the hydraulic ram pump*', University of Warwick Department of Engineering

Joukowsky J.N. (1904) 'Water hammer', *Proceedings of the American Waterworks Association*, Vol 24 pp 341-424.

Munson, Okiishi and Huebsch (2009) *Fundamentals of fluid mechanics* 6th ed. 978-0470-26284-9, John Wiley & Sons, Inc

'Rife hydraulic water rams', (1985) Rife Hydraulic Engine Manufacturing Co.

Smith, W. B. (2017) '*Home-made hydraulic ram pump for livestock water*', Clemson University Extension Services

Swamee, P. K., and Jain, A. K. (1976) 'Explicit equations for pipe-flow problems' J. *Hydr. Div.,* ASCE, 102(5), 657-664.

Young, B. (1997) 'Design of homologous ram pumps', J. *Fluids Eng.* June 1997, 119(2): 360-365

8 APPENDICIES

8.1 Matlab Hydraulic Ram Pump Design Evaluator

The code below can be used to determine the minimum and maximum operating characteristics of a specific ram pump design. If the model determines the ram pump design is not feasible, the code will output whether the fall height or the amount of supply flow is the limiting factor on pump performance. The additional assumptions used in the code are listed in the first block of comments.

```
% Ram Pump Design Evaluator
% Max Pawlick 8/29/21
% Assumes density of water is 1000kg/m^3 and kinematic viscosity is 0.0000011384; % m^2/s
% Assumes acceleration due to gravity is 9.8 m/s^2
% Assumes the bulk modulus of water is 2.19*10^9 pa
%% Collect Data From User
promptyUnit = 'What unit system is preferred [Metric or English] \n';
%determine unit system for data entry
Unit=input(promptyUnit,'s');
if strcmpi(Unit,'Metric')
% collect data in metric units
promptyM = 'What is the Youngs Modulus of the drive pipe material? [pascals] \n';
promptWThick = 'What is the wall thickness of the drive pipe? [mm] \n';
promptARough = 'What is the absolute roughness of the drive pipe material? [mm] \n';
promptDH = 'What is the inner diameter of the drive pipe? [mm] \n';
promptDPipeL = 'What is the length of the drive pipe? [m] \n';
promptFH = 'How much fall height is available? [m] \n';
promptQin = 'What is the minimum available flowrate of the water source? [liters/minute] \n';
promptLH = 'How much lift height does the pump need to overcome? [m] \n';
promptKval = 'What is the estimated total K-Value of the bends in the drive pipe and the waste valve?
(generally between 10 and 15) [-] \n';

yMod=input(promptyM);
wThick=input(promptWThick)/1000; % mm to m
e=input(promptARough)/1000; % mm to m
Dh=input(promptDH)/1000; % mm to m
dpLength=input(promptDPipeL);
supplyFlow=input(promptQin); %kept in liters per minute
liftHeight=input(promptLH);
fallHeight=input(promptFH);
kVal=input(promptKval);

elseif strcmpi(Unit,'English')

promptyM = 'What is the Youngs Modulus of the drive pipe material? [psi] \n';
promptWThick = 'What is the wall thickness of the drive pipe? [inches] \n';
promptARough = 'What is the absolute roughness of the drive pipe material? [inches] \n';
promptDH = 'What is the inner diameter of the drive pipe? [inches] \n';
promptDPipeL = 'What is the length of the drive pipe? [feet] \n';
promptFH = 'How much fall height is available? [feet] \n';
promptQin = 'What is the minimum available flowrate of the water source? [Gallons/minute] \n';
promptLH = 'How much lift height does the pump need to overcome? [feet] \n';
promptKval = 'What is the estimated total K-Value of the bends in the drive pipe and the waste valve?
(generally, between 10 and 15) [-] \n';

yMod=input(promptyM)*6894.76; % psi to pa
wThick=input(promptWThick)*2.54/100; % inches to meters
```

```
e=input(promptARough)*2.54/100; % inches to meters
Dh=input(promptDH)*2.54/100; % inches to meters
dpLength=input(promptDPipeL)/3.28; % feet to meters
supplyFlow=input(promptQin)*3.785; % gallons to liters
liftHeight=input(promptLH)/3.28; % feet to meters
fallHeight=input(promptFH)/3.28; % feet to meters
kVal=input(promptKval);

else
    error('Did not recognize input for unit system, enter "Metric" or "English"')
end

g=9.8; %acceleration due to gravity
row=1000; %density of water
vK= 0.0000011384; % kinematic viscosity m^2/s assuming water temp of 15 degrees Celsius
bMW=2.19*10^9; % The bulk modulus of water
%% Complete preliminary calculations
hOverL=fallHeight/dpLength;
deliveryPressure=row*g*liftHeight;
minSpikeP=deliveryPressure*1.3;
waveVel=(1/(row*((1/(bMW))+(Dh/(yMod*wThick)))))^0.5;
minSpikeVel=minSpikeP/(row*waveVel*0.8);
aveV=minSpikeVel*0.7; % assuming the average drive pipe velocity while the flow accelerates is 70%
Re=aveV*Dh/vK; % Average Reynolds number while the flow accelerates. Used to estimate the average Hazen
Williams friction coefficient.
c=(log10((e/(3.7*Dh))+(5.75/(Re^0.9))))/(-0.0432*Dh^0.0093*(Re*vK)^0.074))^1.08; %Calculates the average
Hazen Williams coefficient
Fp1=e/(3.7*Dh); % Fp (1,2,and 3)are used to calculate the resistance of the pipe during turbulent flow
Fp2=5.74*(vK/Dh)^(0.9);
Fp3=1/(2*Dh);
FpL=64*vK/(2*Dh^2); %Represents the resistance of the pipe during laminar flow
Fv=(kVal)/(2*dpLength); %Represents the resistance of the bends and waste valve

%% Set up and solve the equations of drive pipe flow
tspan = linspace(0,7,200);  % This assumes the spike velocity will be reached in 7 seconds
% tspan may need to be extended for drive pipes larger than 3 inches with
% low fall height to length ratios
tspanL=linspace(0,2,100); % Assumes the flow will transition to turbulent within 2 seconds
initialvaluesL=[0,0]; %Assumes the flow is stationary at the start of each cycle
[tL,xL]=ode45(@(tL,xL) fL(tL,xL,hOverL,FpL,Fv),tspan,initialvaluesL); %Solves for flow translation and
velocity during laminar flow
ReL=xL(:,2)*Dh/vK; %Calculates the Reynolds number for the solution.
turbLoc=max(find(ReL>3000,1)); %Determines the point where the flow transitions to turbulent
initialvalues=[xL(turbLoc,1),xL(turbLoc,2)]; %Defines the initial values from the laminar solutions at
the point of turbulence
[t,x]=ode45(@(t,x)  f(t,x,hOverL,Fp1,Fp2,Fp3,Fv),tspan,initialvalues);  %Solves  for  the  velocity  and
distance traveled by the flow over time
t=t+tL(turbLoc); %Adds the time it took the flow to become turbulent to the turbulent time vector
aLength=size(t);
depth=aLength(1);

%% Calculate the amount of fall height needed for various spike velocities
hlPressure=zeros(depth,1);
for hwIndex=2:depth
    numericVel=(x(hwIndex-1,2)+x(hwIndex,2))/2; %Calculates the average velocity over the time interval
    deltaX=x(hwIndex,1)-x(hwIndex-1,1); %Calculates the distance traveled during the time interval
```

```
    numRe=Dh*numericVel/vK; %Calculates the average Reynolds number during the time interval

    if numRe>3000 %Turbulent flow
        f_darcy(hwIndex,1)=0.25/(log10(Fp1+Fp2/(numericVel^(0.9))))^2; %Swamee-Jain equation for Darcy
friciton factor

    else %Laminar flow
       f_darcy(hwIndex,1)=(64/numRe); %Darcy Weisbach equation
    end
    hlPressure(hwIndex,1)=f_darcy(hwIndex,1)*row/2*numericVel^2/Dh*deltaX; %Darcy-Weisbach equation for
pressure drop

    % In the line below, to account for waste valve loss row*g on right hand side used to convert meters
head to pascals

hlPressure(hwIndex,1)=hlPressure(hwIndex,1)+(kVal*numericVel^2)/(2*g)*(row*g);
    %to account for head loss from previous increments
     hlPressure(hwIndex,1)=hlPressure(hwIndex,1)+hlPressure(hwIndex-1,1);
end
velocityPressure=(row/2)*x(:,2).^2; %Represents the velocity pressure for each possible velocity
totalHeadRequired=hlPressure+velocityPressure; % Adds velocity pressure to frictional losses to determine
total head required

%% Calculating Possible Performance data
frequency=60./(t+(dpLength/waveVel)*2); %Calculates the maximum amount of times the pump will cycle per
minute
wasteVolumePerCycle=x(:,1)*(pi/4*Dh^2); %Converts the linear distance traveled by the flow to volume
wasteVolumePerMinute=wasteVolumePerCycle.*frequency;
wasteVLPM=wasteVolumePerMinute*1000; %converts from cubic meters to liters
litersIn=wasteVLPM/(1-(fallHeight/liftHeight)); %This adds the maximum possible delivery flow to
determine the total flowrate required
%% Calculating Feasible Performance Data
possibleVelsLogic1=max(find(litersIn<supplyFlow)); %Determines if there is enough supply flow for each
possible spike velocity
possibleVelsLogic2=max(find(totalHeadRequired<(fallHeight*row*g)));%Determines if there is enough head
pressure for each possible velocity
if possibleVelsLogic1<possibleVelsLogic2 %Determines whether head pressure or supply flow is limiting
the spike velocity
    velLoc=possibleVelsLogic1;
    diaLimiting="supply flowrate. \n";
else
    velLoc=possibleVelsLogic2;
    diaLimiting="fall height. \n";
end
posibleVels=x(1:velLoc,2); %Determines what spike velocities are possible for the system
maxPV=max(posibleVels); % Determines the maximum possible spike velocity
if minSpikeVel>maxPV %Determines if the maximum possible velocity is greater than the velocity required
to pump water
    outDiaOne=fprintf("Not feasible. The limiting factor of the system is " + diaLimiting );
else
  % calculates the mass of the valve wafer required to cause the minimum spike velocity
    valveMinMass=(row*(pi/4)*Dh^2*minSpikeVel^2)/g;
    valveMaxMass=(row*(pi/4)*Dh^2*maxPV^2)/g;
%calculates the min and max spike pressure the pump will have to handle in pa
    spikePressureMin=waveVel*row*minSpikeVel;
    spikePressureMax=waveVel*row*maxPV;
```

```
%% Generating Output Report
if strcmpi(Unit,'Metric')

   outDiaOne=fprintf("Feasible \n The pump can operate between spike velocities of " + num2str(minSpikeVel)
+ " and " +num2str(maxPV) + " meters/second. ");
      outDiaTwo=fprintf("\n This will produce spike pressures the pump needs to absorb between " +
num2str(spikePressureMin) + " and " +num2str(spikePressureMax)+ " pa. " );
   outDiaThree=fprintf("\n A circular waste valve wafer would need a mass between " + num2str(valveMinMass)
+ " and " +num2str(valveMaxMass)+ " kilograms to produce this range of spike velocities. \n");
     outDiaFour=fprintf(" Increasing the spike velocity, pressure, and valve weight will increase the
amount of flow delivered, but may cause strain on the pump materials. \n");
    outDiaFive=fprintf(" The power of the system is limited by the available " + diaLimiting);
else
    minSpikeVel_E=minSpikeVel*3.28; % meters to feet
    maxPV_E=maxPV*3.28; % meters to feet
    spikePressureMin_E=spikePressureMin/6894.76; % pa to psi
    spikePressureMax_E=spikePressureMax/6894.76; % pa to psi
    valveMinMass_E=valveMinMass*2.205; % kg to lb
    valveMaxMass_E=valveMaxMass*2.205; % kg to lb

  outDiaOne=fprintf("Feasible \n The pump can operate between spike velocities of " + num2str(minSpikeVel_E)
+ " and " +num2str(maxPV_E) + " feet/second. ");
      outDiaTwo=fprintf("\n This will produce spike pressures the pump needs to absorb between " +
num2str(spikePressureMin_E) + " and " +num2str(spikePressureMax_E)+ " psi. " );
  outDiaThree=fprintf("\n A circular waste valve wafer would need a mass between " + num2str(valveMinMass_E)
+ " and " +num2str(valveMaxMass_E)+ " pounds to produce this range of spike velocities. \n");
     outDiaFour=fprintf(" Increasing the spike velocity, pressure, and valve weight will increase the
amount of flow delivered, but may cause strain on the pump materials. \n");
    outDiaFive=fprintf(" The power of the system is limited by the available " + diaLimiting);


end
end
%% Differential Equation to calculate laminar flow acceleration
function rkL=fL(tL,xL,hOverLF,FpFL,FvFL)
            g=9.8;
            rkL=[xL(2);g*hOverLF-FpFL*(xL(2))-FvFL*(xL(2))^2];
       end
%% Differential Equation to calculate turbulent flow acceleration
  function rk=f(t,x,hOverLF,Fpf1,Fpf2,Fpf3,FvF)
            g=9.8;
            rk=[x(2);g*hOverLF-0.25/((log10(Fpf1+Fpf2/(x(2)^0.9))))^2*Fpf3*x(2)^2-FvF*(x(2))^2];
        end
```

Comparison of green and brown coconut husks as a packing material in an anaerobic filter

Nicola Brown
School of Food and Advanced Technology, Massey University,
Palmerston North, New Zealand
N.Brown@massey.ac.nz

Zoe Daborn
School of Food and Advanced Technology, Massey University,
Palmerston North, New Zealand
dabornzoe@gmail.com

John Edwards
School of Food and Advanced Technology, Massey University,
Palmerston North, New Zealand
J.Edwards@massey.ac.nz

Shazwani Shamsulgafar
School of Food and Advanced Technology, Massey University,
Palmerston North, New Zealand
wanieaimi@gmail.com

ABSTRACT: *Septic tanks can become overloaded overtime due to increases in the size of households or the build-up of sludge. This results in the wastewater spending less time within the tank and therefore a reduced level of treatment. One solution to enhance treatment is to add an anerobic filter after the existing septic tank. The anaerobic filter requires media for the establishment of a biofilm, and the use of coconut husks was identified as a possibility due to their abundance. Both green and brown coconut husks were imported from Tonga and tested in laboratory scale anaerobic filters treating synthetic wastewater. The treatment performance was monitored in terms of the chemical oxygen demand (COD) which is a measure of organic strength. There was also potential for organic material to leach out of the coconut husks, so additional testing was done to evaluate this. It was found that four times more COD was leached from the green coconut husks showing that brown coconut husks were the better choice. The brown coconut husk reactor reduced the COD concentration by 49 %. This study has indicated that there is value in examining the feasibility of implementing an anaerobic filter using brown coconut husks to enhance wastewater treatment from septic tanks. Further research should focus on examining whether any nutrients are released from the husk and then practical considerations such as the scale needed for a household and maintenance requirements.*

KEYWORDS: *Anaerobic filter, Coconut husk, Septic tank effluent, Wastewater treatment*

1 INTRODUCTION

Many Pacific Island communities do not have centralised wastewater treatment facilities with the exception of some urban areas (Secretariat of the Pacific Regional Environment Programme, 2020). For example, in Tonga there are no centralised wastewater treatment facilities, and 94 % of households use septic tanks (Tonga Statistics Department, 2021). A recent survey showed that some septic tanks had not been emptied in 15 years (Radio New Zealand, 2020). This overloading and sludge build-up means that there is

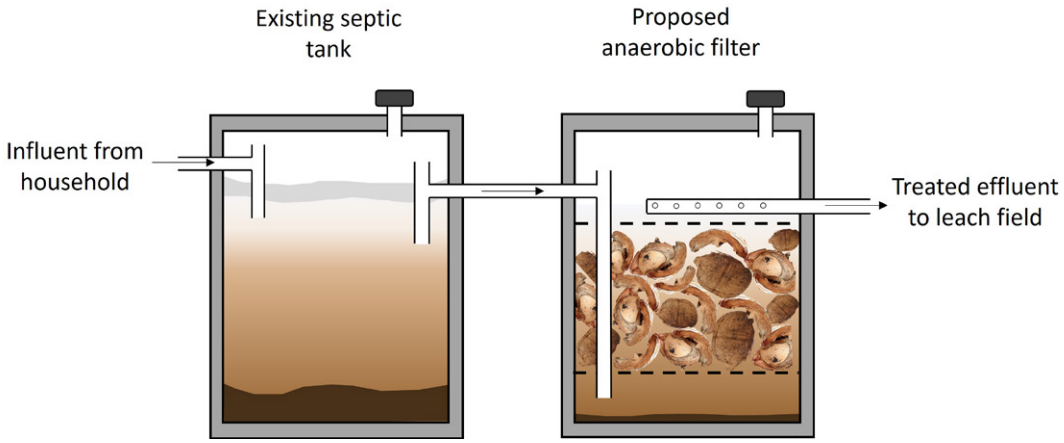

Figure 1: *Existing septic tank followed by proposed anaerobic filter. Image adapted from de Oliveira Cruz et al.* (2019)

less time for the wastewater to be treated in the septic tank. This reduced treatment can have negative consequences when the wastewater is discharged to the environment. This poses not only a direct health risk to the people, but it can also pollute the surrounding sea and impact marine life.

A solution to this problem could be to install an anaerobic filter downstream from the septic tank. Anaerobic filters are very effective at polishing effluent, without producing large amounts of sludge or need for maintenance (Toerien and Hattingh, 1969). These systems require a surface for microorganisms to attach to and grow in the form of a biofilm (Toerien and Hattingh, 1969). Ideally the packing material is locally available at low cost and has a large surface area for biofilm establishment. Many different types of media have been used in anaerobic filters including locally available rock or gravel (Lopez-Lopez et al., 2013; Kaetzl et al., 2013; Heredia et al., 2022), woodchips (Kaetzl et al., 2013), and coconut shells or husks (Heredia et al., 2022; de Oliveira Cruz et al., 2019; Silvia et al., 2015; de Oliveira Cruz et al., 2013). Coconut husks offer a potential solution due to the abundance of coconuts in the Pacific and the large surface area due to the fibrous nature of the husks.

Figure 1 gives an overview of the proposed system. The effluent from the existing septic tank passes into the anaerobic filter which is full of coconut husks. A biofilm grows on the husks and treats the wastewater. The treated effluent then leaves the anaerobic filter and can be disposed of as usual.

There have been other wastewater treatment systems where microbial growth is attached to coconut fibre-based material. Examples include the use of woven and non-woven coir geotextiles (Salim et al. 2020).

Coconuts can be harvested at different stages of their development depending on the end use of the coconut. If the aim is to maximise the amount of coconut water, they are harvested green or less mature, whereas they are harvested brown or fully mature if the focus is on coconut flesh. Previous studies on using coconut husks or shells within an anaerobic filter have used dried green husks (de Oliveira Cruz et al., 2019) or coconut shells (Silvia et al., 2015; de Oliveira Cruiz et al., 2013). Coconuts are typically harvested when brown in Tonga, and it is not currently known whether the different age of the coconut husks has an impact on their effectiveness as a packing material in an anaerobic filter.

The purpose of this study is to determine whether this system would be appropriate for use in Tonga. This is done by trying to closely mimic the conditions found in Tonga and analysing the treatment performance and stability of the anaerobic filter when comparing green and brown coconut husks. The treatment performance is measured in terms of chemical oxygen demand (COD), and pH is used as a measure of stability.

2 METHODOLOGY

This section first describes the two types of coconut husks used in the work (Section 2.1). The anaerobic filter reactor set-up and conditions are described (Section 2.2) followed by how the reactors were operated (Section 2.3). The experiments used to examine the release of COD from the coconut husks are described (Section 2.4). Finally, in Section 2.5, details on the sample analysis are given.

2.1 Coconut husks used in this study

There are two types of coconut husk evaluated in this study. These are green coconut husks and brown coconut husks. The green and brown coconut husks were sourced from Tonga and sent to our laboratory in New Zealand. Photographs of each type of coconut husk are shown

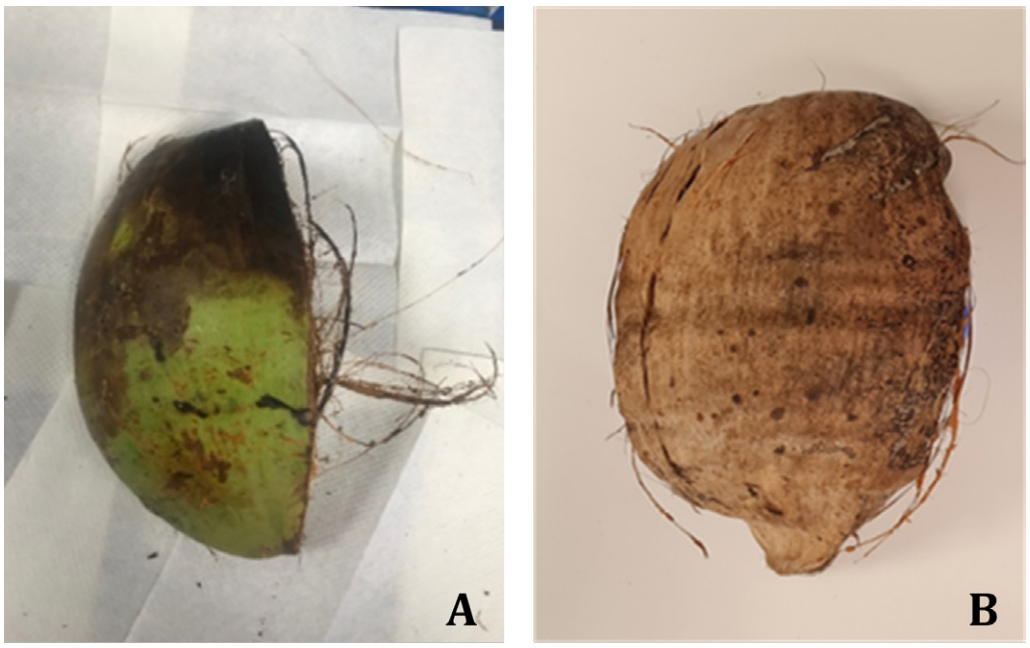

Figure 2: *Photographs of the different types of coconut husks sourced for this project (A – green coconut husk; B – brown coconut husk)*

Table 1: *Characteristics of the coconut husks*

Coconut husk type	Number of measurements	Mean length (mm)	Mean width (mm)	Mean depth (mm)	Mean weight (g)	Moisture content (%)
Green husk	1.06	399	100	30	345	0.863
Brown husk	7	230	100	30	96	35

in Figure 2, and information on their moisture content, weight and size is given in Table 1.

While the dimensions of the green and brown coconut husk pieces are similar, the weight of the green coconut husk is significantly higher due to its moisture content (Table 1). The aging process from green to brown has resulted in moisture loss from the husk.

2.2 Design of the reactors and experimental conditions

Laboratory scale reactors were constructed to mimic an anaerobic filter. The set-up consisted of a series of 20 L containers as shown in Figure 3. The feed was then pumped into the bottom of the anaerobic filter. Further detail of the filter is shown in Figure 4. There was a perforated plate towards the bottom and towards the top of the reactor to keep the pieces of coconut husk in place. The feed flowed up through the reactor and exited near the top of the reactor. A final container then collected the effluent and there was a sampling valve fitted to collect samples.

Two of the set-ups shown in Figure 3 were constructed. One was used for the green coconut husks and the other was used for the brown coconut husks.

Temperature

The mean temperature in Tonga was reported to be 24.3 °C in 2020 (Climate data.org, 2021). Our collaborators in Tonga from the Ministry of Lands and Natural Resources also measured the temperature of two septic tanks and found them to be 19.5 °C and 20 °C (A. Pale, personal communication, 11 June 2021). It was therefore decided that the reactors would be operated at approximately 20 °C.

Synthetic wastewater

Synthetic wastewater was used as the influent into the anaerobic filters and was designed to mimic the wastewater

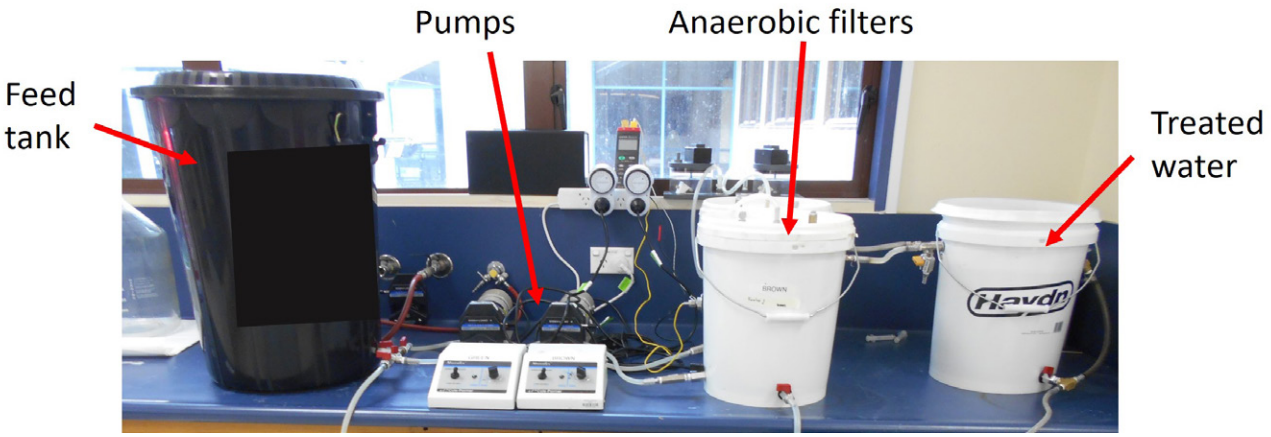

Figure 3: Photograph of the setup for the anaerobic filters

from a domestic dwelling which had already been treated in a septic tank. The synthetic wastewater used in this study was from Rodgers et al. (2010). The synthetic wastewater was found to have a chemical oxygen demand (COD) concentration of 690 mg/L and an average pH of 7.4. The synthetic wastewater was then further diluted to achieve the desired COD concentration.

Feeding regime

The conditions that the system would experience in Tonga were used to determine the feeding regime. Information from our collaborators from the Ministry of Lands and Natural Resources indicated that often residents do not stay in their homes during the day and therefore there is little flow to septic tanks at that time (A. Pale, personal communication, 13 July 2021). The feeding of the reactors was therefore set to mimic the residents' production of wastewater by having the pump turn on for a period of time in the morning and evening. While this does not account for wastewater production throughout the day, it is more representative than a constant feed rate.

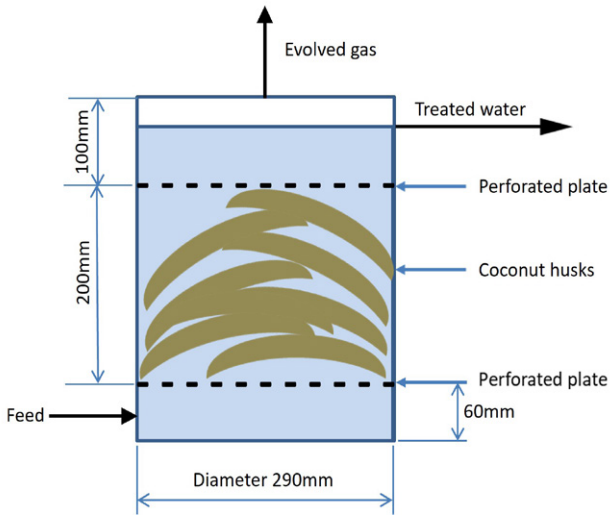

Figure 4: Diagram showing the detail of how the anaerobic filters were constructed

Anaerobic filters can operate at hydraulic retention times (HRT) of 12 to 96 hours (Young and Yang, 1989). The flow rate of the pump was based on achieving a HRT of 16.8 hours based on the study by de Oliveira Cruz et al. (2019). The different-sized pieces of coconut husk resulted in slightly different flow rates in order to achieve the same retention time in both reactors. The green coconut husk reactor had 7.8 L of fluid and therefore the reactor was fed with approximately 5.6 L morning and evening over a one-hour period. The brown coconut husk reactor had 8.8 L of fluid and therefore the reactor was fed with approximately 6.3 L morning and evening over a one-hour period. The resulting organic loading rate for both reactors was 0.18 g COD/L/d.

2.3 Operation of reactors

Start-up period

During the start-up period microorganisms within the reactor were established. To do this, first a source of microorganisms is needed which was collected from a dairy farm effluent pond. This contained anaerobic bacteria which would be able to establish within the reactor. The pieces of coconut husk were placed in the dairy farm pond water for 15 minutes and then taken out and placed in the reactor. Note that this would not be needed if this was downstream of a septic tank because the effluent from the septic tank would provide these microorganisms.

When feeding of the synthetic wastewater began, it was at a lower COD concentration and then slowly increased to 125 mg/L. To monitor the stability of the reactor, the

Table 2: Amount of coconut husk used in the COD release experiments

Coconut husk type	Wet weight (g)	Dry Weight (g)	Moisture Content (%)
Green husk	257	36	86
Brown husk	150	98	35

pH was measured. The concentration of the synthetic wastewater was slowly increased if the pH was stable.

Evaluation period

Once the reactor reached a COD concentration of 125 mg/L, then the evaluation period started. During the evaluation period, the COD concentration remained constant. Data were then gathered to establish the performance of the reactors and compare green and brown coconut husks.

2.4 COD release from coconut husks

An additional set of experiments focused on testing whether any COD was released from the coconut husk into the water. As coconut husk is an organic material, it is possible that carbon and nutrients such as nitrogen and phosphate could be released as the coconut husk breaks down. It is important to examine this aspect to enable the performance of different types of husks to be compared.

For these experiments, one piece of husk was placed in a container with 6 L of water. The containers were closed to minimise evaporation. Details of the weight and moisture content for each type of coconut husk are given in Table 2.

The liquid was monitored for COD and pH. Measurements for nitrate and phosphate were also taken towards the end of the experiment to determine if nutrients were being released from the coconut husks.

2.5 Sample analysis

Chemical oxygen demand (COD)

There are many organic substances which can have an adverse effect on the environment. This adverse effect is due to the oxygen required to break down these compounds. In order to measure the pollution potential of waste, the amount of oxygen which is consumed to break down the substances needs to be measured. The analytical method used in this study was the COD.

The COD analysis was conducted using the Thermo Scientific COD test kits and measuring the colour change using a spectrophotometer.

pH

There are a wide range of microorganisms involved in reducing COD in an anaerobic system. These microorganisms can be separated into two types. The first type are acid producers, and they start the process by breaking down the organic material into organic acids. The second type of microorganisms break down the organic acids into methane ($CH4$) and carbon dioxide ($CO2$) which are gases, and this ultimately results in the COD being reduced from the liquid. This process is summarised in Figure 5.

Both groups of microorganisms need to work together to reduce the COD. If the acid producing organisms do not break down the organic material, then there is no food for the methane producing microorganisms. This can also lead to a reduction in the pH due to the build-up of acids. This can be an issue as the methane producing microorganisms are sensitive to changes in pH, and they prefer a pH above 6.5 (Young and Yang, 1989). By measuring the pH, the process can be monitored to ensure that both sets of microorganisms are working effectively.

The pH was measured using a probe and a handheld meter. The probe was calibrated using a two-point calibration before measurements were taken.

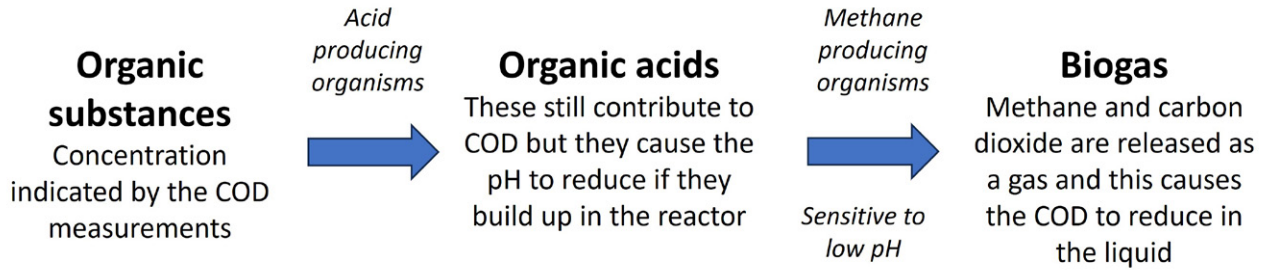

Figure 5: The biological processes occurring within the anaerobic filter

Nitrate and phosphate

It is possible that as the coconut husk breaks down, nutrients like nitrate and phosphate are released. It is important to analyse for these components as these nutrients can have adverse effects on the environment. Samples from the feed and the anaerobic reactors were analysed to determine if there was an increase in nitrate and phosphate. Anaerobic processes do not typically achieve high nutrient removal, so no significant change between influent and effluent would be expected if there is no leaching from the coconut husk.

Prepared Hach test kits were used to analyse samples for nitrate and phosphate.

3 RESULTS AND DISCUSSION

3.1 Reactor performance

The key parameter of interest for this study is the COD reduction within the reactor. First there is a period where the reactor is being slowly started up before it reaches the full COD concentration in the feed. In this study the start-up period was done slowly to ensure that the reactor remained stable. The purpose of this study was to see if a stable reactor could be maintained and to evaluate the COD reduction, therefore a cautious approach was taken to start-up.

After the start-up period, a steady COD concentration was used in the feed, and the COD removal in the reactors could be determined. The data summarised in Figure 6 show the percentage COD removal once start-up had been completed for the green and brown husk reactors.

The average percentage COD removal for the green coconut husks was 21 % (Figure 6) with an average effluent concentration of 103 mg/L. For the brown coconut husks, the performance was better with an average COD removal of 49 % (Figure 6) and an average effluent concentration of 64 mg/L. Prior work by de Oliveira Cruz et al. (2019) reported a COD removal efficiency of 52 % which is similar to the performance of the brown coconut husk reactor. The work by de Oliveira Cruz et al. (2019) was conducted using dried green coconut husks. It is possible that the drying process led to the coconut husks behaving in a similar way to the brown coconut husk rather than the fresh green coconut husks.

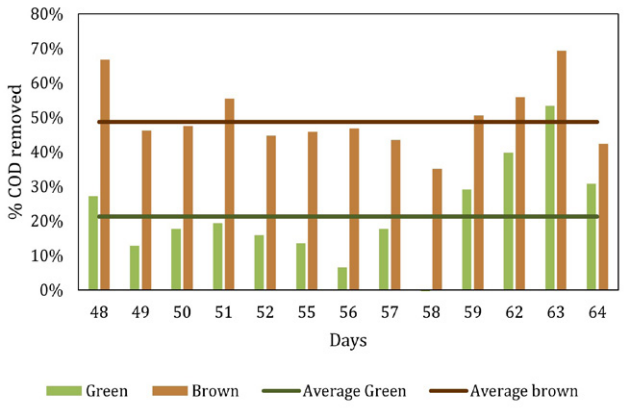

Figure 6: Green and brown coconut husk reactor COD removal performance during the evaluation stage of the experiment

3.2 pH of the reactors

Throughout the experiments, the pH was monitored. Typically, healthy anaerobic reactors have a pH above 6.5 (Young and Yang, 1989). Figure 7 shows the pH throughout the experiments. During the start-up phase, the pH was more likely to drop below 6.5; however, during the evaluation period, the pH was more stable. The average pH during the evaluation period was 6.49 for the green coconut husk reactor and 6.60 for the brown husk.

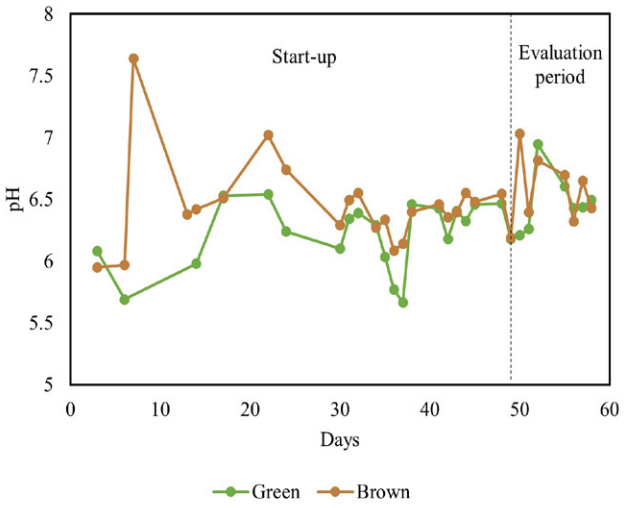

Figure 7: pH of the green and brown coconut husk reactors. The dotted line shows when the evaluation period started

3.3 COD release from coconut husks

The leaching tests were conducted to determine how much COD was released from the coconut husks as this would contribute to the COD in the effluent. Figure 8 shows why this is important. There is a certain amount of COD entering the reactor in the feed. Some of this COD will be consumed by the microorganisms in the biofilm. There will also be some untreated COD which they do not consume which will pass out of the reactor in the effluent. As the coconut husk is an organic material, it will slowly break down and, as a result, some COD will be released out of

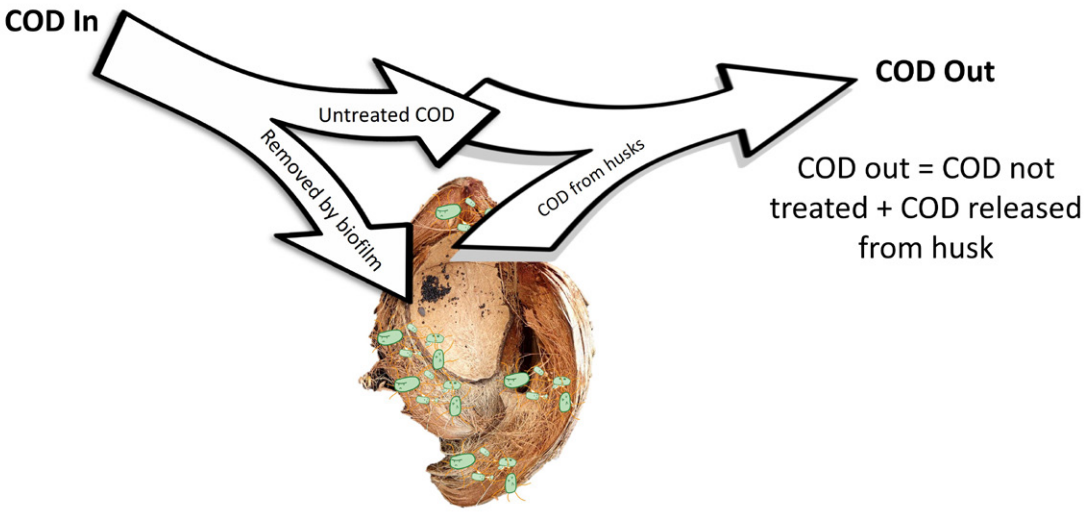

Figure 8: *Existing septic tank followed by proposed anaerobic filter. Image adapted from de Oliveira Cruz et al.* (2019)

the husk into the surrounding water which is referred to as leaching. The COD which is leached from the husk then passes out of the reactor with the effluent. This means that the effluent contains a combination of the COD which is not removed from the feed plus some COD which has been leached from the coconut husks.

It was expected that there would be a difference in the COD released from the green and brown coconut husks. The brown husk has been naturally matured over time, and it is likely that some of the COD that it once contained has already been released in the environment.

The pieces of coconut husk tested were different sizes; to account for this, the results are presented as the amount of COD leached per amount of dry coconut husk (Figure 9). Higher values mean that more COD is being released from the coconut husk and therefore the COD removal happening within the reactor may be masked by the large amount of COD being released.

As expected, there was more COD released from the green husk compared to the brown husk (Figure 9). The COD values do fluctuate, and this is probably due to microorganisms growing in the reactor and on the surface of the husk which would consume some of the COD. The maximum COD values for the green and browns husks were 71.3 and 17.5 mg COD/mg dry husk, respectively. This means that more than four times the amount of COD was leached for the green husk. This confirms the expectation that the brown coconut has already started to break down during the ageing process.

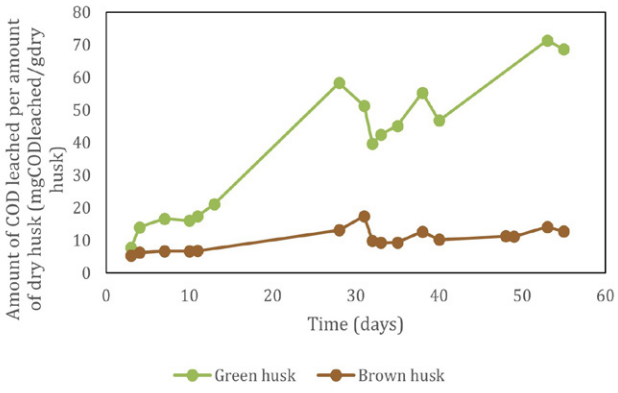

Figure 9: *COD released from the coconut husks in the leaching experiments. Results are presented as the COD per amount of dry coconut husk to correct for different amounts of coconut husk in the test*

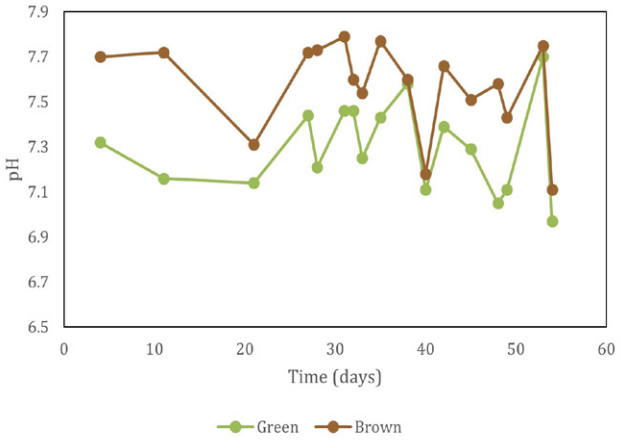

Figure 10: *The pH of the water in the leaching experiments*

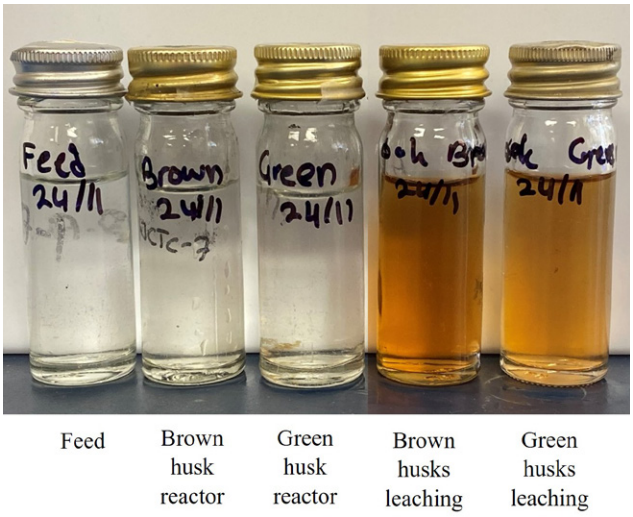

Figure 11: *Photograph of samples from each trial to compare the colour*

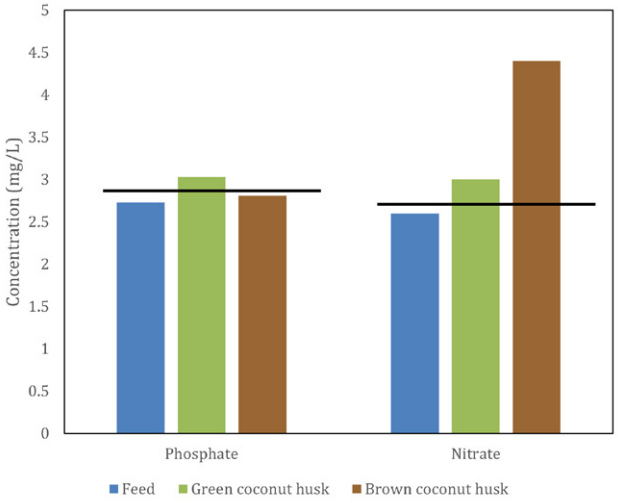

Figure 12: *Phosphate and nitrate concentration in the feed and each of the coconut husk reactors. The black line is to allow easy comparison with the feed concentration.*

The pH of the liquid during the leaching experiment was also of interest (Figure 10). For both the green and brown coconut husks, the pH was above 7 which is not acidic and should not negatively impact the anaerobic digestion process.

Colour leaching out of the coconut husk was observed in the COD release experiments, so samples were taken from each reactor to compare. As seen in Figure 11, the up flow anaerobic filter reactors did not show a significant amount of colour; however, all of the COD release experiments did. The lack of colour in the anaerobic filters is probably due to dilution from the synthetic wastewater which is colourless and the fact that these reactors were run continuously whereas the leaching trials were batch.

3.4 Nitrate and phosphate release

The results have shown that COD is leached out of the coconut husks, and it is possible that other components are also being leached out of the husks. Particular compounds of interest include nitrogen and phosphorus which could cause adverse effects on the receiving environment. Figure 12 shows the concentration of phosphate and nitrate in the feed and the effluent from the reactors. Significant nutrient removal is not expected in the anaerobic filter, so any changes in the nutrient concentrations are likely to be due to leaching from the coconut husk. The amount of nutrients leached out of the coconut husk can be examined by looking at the difference between the feed and the reactors. The black line in Figure 12 assists with this. If the bars are above the black line, then this indicates that nutrients may have been released by the coconut husk. The only measurement which suggests that there may be some leaching is the nitrate value for the brown coconut husk reactor. However, it should be noted that this is based on very limited data. More data would be required before a conclusion can be drawn.

3.5 Implications of the findings

The performance of the anaerobic filter is determined by a combination of COD being treated by the microorganisms in the reactor and COD being released by the coconut husk back into the water. The final effluent COD concentration for the brown coconut husk reactor was 64 mg/L. To put this value in perspective, one manufacturer reported that package sewage treatment systems, which are small-scale wastewater treatment plants, are designed to achieve a COD effluent concentration of 75 mg/L (Butlerms, n.d.). Based on the initial findings presented in this report, this level of treatment could be achieved by adding an up flow anaerobic filter using brown coconut husks as the surface for attached growth of microorganisms.

There are several areas which require further work before this technology could be implemented. As already identified, the potential for nutrients to be leached from the coconut husk needs to be examined in more detail. Long-term data are required to determine maintenance requirements. Previous work has shown that coconut shells can be used in an anaerobic filter for two years (Silva et al., 2015), but this would need to be confirmed with coconut husks as the rate of breakdown could be different. Determining the size of a reactor for a household will also be important, but further optimisation of the process by varying the HRT is needed before this can be determined. The stability of the process to handle changes in the COD concentration should also be considered to mimic times when the septic tank does not work as expected or when there is a higher loading due to more occupants of a household than expected.

4 CONCLUSIONS

The potential of an anerobic filter using coconut husks as the attachment media was examined, and both green and brown coconut husks were trialled. It was found that there were two mechanisms simultaneously occurring which determined the effluent concentration. COD was removed due to anaerobic treatment, but COD was also leached from the coconut husk back out into the liquid. The green coconut husk was found to release larger amounts of COD and therefore the reactor did not remove as much COD. The brown coconut husk released less COD and therefore that reactor was able to remove 49 % of the COD overall.

There could be several aspects to focus on in future work. These could include determining the start-up procedure, examining nutrient removal in more detail, conducting work to determine the size of the unit required for a typical Pacific Island household, and gathering long-term data to establish when maintenance is required.

5 ACKNOWLEDGEMENTS

We would like to acknowledge the Government of the Kingdom of Tonga for providing us with a Tonga Government Research Permit. We would also like to thank our collaborators from the Ministry of Lands and Natural Resources in the Kingdom of Tonga for their advice and support throughout this project.

6 REFERENCES

Butlerms (n.d.) '*Sewage parameters* 7: *Chemical oxygen demand* (*COD*)'. Available at: https://butlerms.com/sewage-parameters-7-chemical-oxygen-demand-cod/ (Accessed: 9 December 2021).

Climate data.org (2021) '*Climate*: *Tonga*'. Available at: https://en.climate-data.org/oceania/tonga-97/ (Accessed: 9 December 2021).

de Oliveira Cruz, L.M.O., Gomes, B.G.L.A., Tonetti, A.L., and Figueiredo, I.C.S. (2019) 'Using coconut husks in a full-scale decentralized wastewater treatment system: The influence of an anaerobic filter on maintenance and operational conditions of a sand filter', *Ecological Engineering,* 127, pp. 454-459.

de Oliveira Cruz, L.M.O., Stefanutti, R., Filho, B.C., and Tonetti, A.L. (2013) 'Coconut shells as filling material for anaerobic filters', *SpringerPlus,* 2, pp. 655.

Heredia, R.M., Layedra-Almeida, A.P., Torres, Y., and Toulkeridis, T. (2022) 'Evaluation of a microbial consortium and selection of a support in an anaerobic reactor directed to the bio-treatment of wastewater of the textile industry', *Sustainability,* 14, pp. 8889.

Kaetzl, K., Lubken, M., Gehring, T., and Wichern, M. (2013) 'Efficient low-cost anaerobic treatment of wastewater using biochar and woodchip filters', *Water,* 10, pp. 818.

Lopez-Lopez, A., Albarran-Rivas, M.G., Harnandez-Mena, L., and Leon-Becerril, E. (2013) 'An assessment of an anaerobic filter packed with a low-cost material for treating domestic wastewater', *Environmental Technology*, 34, pp. 1151-1159.

Pale, A. (2021) personal communication, 11 June.

Radio New Zealand (2020) '*The trouble with talking about toilets in Tonga*'. Available at: https://www.rnz.co.nz/audio/player?audio_id=2018750503 (Accessed 23 October 2021).

Rodgers, M., Walsh, G., and Healy, G. (2010) 'Different depth intermittent sand filters for laboratory treatment of synthetic wastewater with concentration close to measured septic tank effluent', *Journal of Environmental Science and Health,* Part A, 46, pp. 80-85.

Salim, M.K., Linta, N.P., Roush, A.H.M., Ismail, M., and Nazim, F. (2020) 'Treatment of wastewater using woven and non woven coir geotextiles', *International Journal of Creative Research Thoughts*, 8(5), pp. 1502-1507.

Secretariat of the Pacific Regional Environment Programme (2020) '*State of the environment and conservation in the Pacific Islands*: 2020 *regional report*: *Indicators* 31 – *access to and quality of sewage treatment*'. Available at: https://library.sprep.org/content/state-environment-and-conservation-pacific-islands-2020-regional-report-indicators-31 (Accessed 09 June 2021).

Silva, J.C.P., Tonetti, A.L., Leonel, L.P., and Costa, A. (2015) 'Denitrification on upflow-anaerobic filter filled with coconut shells (Cocos nucifera)', *Ecological Engineering,* 82, pp. 474-479.

Toerien, D.F. and Hattingh, W.H. (1969) 'Anaerobic digestion I. The microbiology of anaerobic digestion', *Water Research,* 3(6), pp. 385-416.

Tonga Statistics Department (2021) '*Population and housing census* 2021'. Available at: https://tongastats.gov.to/census-2/population-census-3/ (Accessed 07 October 2022).

Young, J.C. and Yang, B.S. (1989) 'Design considerations for full-scale anaerobic filters', *Research Journal of the Water Pollution Control Federation,* 61(9/10), pp. 1576-1587.

JOURNAL OF
HUMANITARIAN
ENGINEERING

SUBMISSION GUIDELINES

All paper submissions for the *Journal of Humanitarian Engineering* are to be submitted electronically via the JHE website: http://www.ewb.org.au/jhe/. Authors are required to register and submit their paper by following the 'Register' link on the home page. All submission enquiries can be directed to the Editorial Team: journal@ewb.org.au

Submission style and templates: Please download the paper template which can be found in the 'Author Guidelines' heading in the 'About' section on the JHE website: http://www.ewb.org.au/jhe/. The template consists of the full formatting instructions required for submission. For ease of editing it is requested that the paper be submitted as a Microsoft Office Word text document (or equivalent with .doc or .docx extension) and that the length of the submission does not exceed 8 pages.

More information is available on the JHE website: http://www.ewb.org.au/jhe/

JOURNAL OF
HUMANITARIAN
ENGINEERING

ABOUT JOURNAL OF HUMANITARIAN ENGINEERING

Humanitarian engineering is about applying and developing technology – not to meet a market or financial opportunity – but to address a real human need. It is about serving a disadvantaged community or group, often overlooked by traditional engineering and technology projects. From poverty alleviation to disability access, humanitarian engineering highlights a new approach to developing and implementing technologies. The JHE was established in 2012 to provide a forum for such research to be published. The JHE is published by the Education and Research arm of Engineers Without Borders (EWB) Australia.

Research that collects dust on shelves or is stored away in the depths of an electronic archive is research that fails to make an impact. Dissemination is key, and this is why the JHE is free to submit to and free to access. This is made possible by a hard-working team of volunteers and generous support from EWB Australia's partners.

We love to receive contributions from all occupations within the sector; practitioners, policy-makers, academics, students and communities themselves. We encourage submissions which focus on the application of engineering and technology for the benefit of disadvantaged communities; topics include, but are not limited to:

- Water, sanitation and hygiene
- Waste treatment
- Appropriate technologies
- Renewable energy
- Disability access
- Affordable housing and construction
- Information and communication technologies
- Humanitarian engineering education / service learning
- Applications of humanitarian engineering in policy and practice

Please note that "humanitarian engineering" is often known by a plethora of other names, some of which include "development engineering", "global engineering", "technologies for development" and "appropriate technologies". We are very happy to receive submissions from all of these fields.

If you are interested in submitting an article but may require some assistance in preparing a submission in English, please contact us (journal@ewb.org.au) as we may be able to support you with authorship mentoring.

And don't forget to follow us on Twitter: @Journal_Hum_Eng